View metadata, citation and similar papers at core.ac.uk

brought to you by CORE

provided by Kent Academic Repository

Kent Academic Repository

Full text document (pdf)

Citation for published version

Komza, Klara and Skinner, Matthew M. (2019) First metatarsal trabecular bone structure in extant hominoids and Swartkrans hominins. Journal of Human Evolution, 131 . pp. 1-21. ISSN 0047-2484.

DOI

https://doi.org/10.1016/j.jhevol.2019.03.003

Link to record in KAR

https://kar.kent.ac.uk/73880/

Document Version

Author's Accepted Manuscript

Copyright & reuse
Content in the Kent Academic Repository is made available for research purposes. Unless otherwise stated all content is protected by copyright and in the absence of an open licence (eg Creative Commons), permissions for further reuse of content should be sought from the publisher, author or other copyright holder.

Versions of research
The version in the Kent Academic Repository may differ from the final published version.
Users are advised to check **http://kar.kent.ac.uk** for the status of the paper. **Users should always cite the published version of record.**

Enquiries
For any further enquiries regarding the licence status of this document, please contact:
researchsupport@kent.ac.uk

If you believe this document infringes copyright then please contact the KAR admin team with the take-down information provided at **http://kar.kent.ac.uk/contact.html**

KAR Kent Academic Repository

University of Kent

First metatarsal trabecular bone structure in extant hominoids and Swartkrans hominins.

Klara Komza [1,2], Matthew M. Skinner [2,3]

[1] Department of Anthropology, University of Toronto, Canada

[2] School of Anthropology and Conservation, University of Kent, Canterbury, United Kingdom

[3] Department of Human Evolution, Max Planck Institute for Evolutionary Anthropology, Leipzig, Germany

Corresponding author:
Klara Komza
Department of Anthropology
University of Toronto
19 Russell St.
Toronto, ON
M5S 2S2
Phone: +1(647)393-8644

Abstract

Changes in first metatarsal (MT1) morphology within the hominin clade are crucial for reconstructing the evolution of a forefoot adapted for human-like gait. Studies of the external morphology of the MT1 in humans, non-human apes and fossil hominins, have documented changes in its robusticity, epiphyseal shape and its articulation with the medial cuneiform. Here, we test whether trabecular structure in the MT1 reflects different loading patterns in the forefoot across extant large apes and humans, and within this comparative context, infer locomotor behaviour in two fossil hominins from Swartkrans, South Africa. Microtomographic scans were collected from the MT1 of Pongo sp. (n=6), Gorilla gorilla (n=10), Pan troglodytes (n=10), Homo sapiens (n=11), as well as SKX 5017 (Paranthropus robustus), and SK 1813 (Hominin gen. sp. indet.). Trabecular structure was quantified within the head and base using a 'whole-epiphysis' approach with medtool 4.2. We found that modern humans displayed relatively higher bone volume fraction (BV/TV) in the dorsal region of each epiphysis and a higher overall degree of anisotropy (DA), whereas great apes showed higher BV/TV in the plantar regions, reflecting dorsiflexion at the metatarsophalangeal (MTP) joint in the former and plantarflexion in the latter. Both fossils displayed low DA, with SKX 5017 showing a hyper-dorsal concentration of trabecular bone in the head (similar to humans), while SK 1813 showed a more central trabecular distribution not seen in either humans or non-human apes. Additionally, we found differences between non-human apes, modern humans, and the fossil taxa in trabecular spacing (Tb.Sp.), number (Tb.N.), and thickness (Tb.th.). While low DA in both fossils suggests increased mobility of the MT1, differences in their trabecular distributions could indicate variable locomotion in these Pleistocene hominins (recognizing that the juvenile status of SK 1813 is a potential confounding factor). In particular, evidence for consistent loading in hyper-dorsiflexion in SKX 5017 would suggest locomotor behaviours beyond human-like toe off during terrestrial locomotion.

Keywords: trabecular bone, Paranthropus, locomotion, bipedalism

1. Introduction[1]

One of the central questions within the study of human evolution is how and when obligate bipedalism emerged. The forefoot is of particular importance in addressing this question because it directly reflects the extent to which a species uses its feet for locomotion (either arboreal or terrestrial) and/or manipulation. The first metatarsal (MT1) has undergone a dramatic transformation, from a digit used primarily for grasping, to a digit used mainly for weight-bearing, stabilization, and propulsion in modern humans (Morton, 1922; Elftman and Manter, 1935; Susman, 1983; Harcourt-Smith and Aiello, 2004). Analysis of the partially preserved OH 8 foot formed a critical aspect of the initial diagnosis of bipedalism in Homo habilis (Day and Napier, 1964; Kidd et al., 1996) and a number of studies have incorporated analyses of forefoot bones to argue for committed terrestrial bipedalism in Australopithecus afarensis (Latimer and Lovejoy, 1990; ; Ward 2002 Ward et al., 2011) and an opposable hallux in Ardipithecus ramidus (Lovejoy et al., 2009; White et al., 2015). Equally intriguing is the recent discovery of the Burtele foot, which is similar in age to A. afarensis but displays a number of characteristics that differentiate it morphologically and suggest two different types of bipedal foot loading in the hominin clade at the same time (Haile-Selassie et al., 2012). This variation in hominin foot bone morphology highlights the importance of understanding the form/function relationship of the MT1 in extant and fossil hominoids and, in particular, whether internal bone structure can provide insights into biomechanical loads experienced by the foot during different types of locomotion. Using a comparative sample of modern humans and non-human apes, this study will address whether trabecular structure within the MT1 is reflective of locomotor mode. Furthermore, we will compare them to fossil hominins from Swartkrans (SKX 5017 and SK 1813) to test hypotheses about hominin locomotion in the Plio-Pleistocene of South Africa.

1.1. Bone functional adaptation

Functional interpretations of fossil hominin locomotion largely vary because of a lack of consensus on the functional significance of various external skeletal features. It remains unclear whether ‘primitive’ features represent non-functional evolutionary vestiges, or if they represent

---

[1] Abbreviations: metatarsophalangeal (MTP); tarsometatarsal (TMT)

functional indicators of locomotor behaviour (Stern and Susman, 1983; Clarke and Tobias, 1995; Ward, 2002; Harcourt-Smith and Aiello, 2004; Zipfel et al., 2009). This issue can be partially addressed by studying aspects of bone that are more responsive to external loading. While articular surfaces indicate the joint positions an element is capable of, internal bone is more likely to show the position in which the element was actually loaded (Ruff and Runestad, 1992; Rafferty and Ruff, 1994; Jacobs, 2000; Rubin et al., 2002; Ruff et al., 2006). Diaphyseal cortical bone has been shown to respond to mechanical stress in the shaft and can be indicative of predominant bending forces experienced during loading (Ruff, 1983; Cowin et al., 1985; Doden, 1993; Carlson, 2005; Ruff et al., 2006). However, its function is likely different over joint articular surfaces, where it becomes significantly thinner. It is also covered by cartilage and often contained within a synovial joint. Conversely, the trabecular bone located subchondrally within epiphyses remodels at a faster rate than cortical bone (Eriksen, 2010), and can provide evidence of in vivo loading that may be more useful at reconstructing predominant joint position and associated behaviors (Hodgskinson and Currey, 1990; Rubin et al., 2002; Mittra et al., 2005; Pontzer et al., 2006; Barak et al., 2011; but see Bertram and Swartz, 1991). However, it should be noted that trabecular bone structure does not always correlate with known locomotor patterns in certain mammals, including mice and several primates (Carlson et al., 2008; Ryan and Walker, 2010; Shaw and Ryan, 2012).

The current study focuses on two main structural properties of trabecular bone: bone volume fraction (BV/TV), which is a measure of trabecular thickness, number, and spacing, and degree of anisotropy (DA), which reflects the degree to which trabecular struts are oriented in the same direction. These parameters account for 87-89% of the variance in the strength of a bone (Young's modulus) (Maquer et al., 2015), have been shown to change in relation to magnitude, frequency, and direction of load in in vivo studies (Lanyon, 1974; Hodgskinson and Currey, 1990; Biewener et al., 1996; Mittra et al., 2005; Pontzer et al., 2006; Barak et al. 2011), and to differ among taxa that employ different modes of locomotion (MacLatchy and Müller, 2002; Ryan and Ketcham, 2002, 2005; Ryan and Shaw, 2012; Scherf et al., 2013; Tsegai et al., 2013, 2017; but see Fajardo et al., 2007; Ryan and Walker, 2010). BV/TV and DA are informative parameters because both are less likely to scale allometrically and have been found to respond to loading in predictable ways. BV/TV is generally higher in areas that experience greater compressive loading, and trabecular orientation adapts to the main axis of joint movement (Biewener et al., 1996; Guldberg et al., 1997; Ryan and Ketcham, 2002; Mittra et al., 2005; Pontzer et al., 2006; Chang et al., 2008; Polk et al., 2008; Harrison et al., 2011; Saparin et al., 2011). Responses in DA and BV/TV to biomechanical stressors have been demonstrated in several classic studies on the mammalian calcaneus (Lanyon, 1973, 1974; Skerry and Lanyon, 1995; Biewener et al., 1996; Skedros et al., 2004, 2012; Sinclair et al., 2013). In animals in which the calcaneus does not touch the ground during locomotion, trabeculae underlying the Achilles tendon were aligned with the compressive and tensile principal direction of stress (Lanyon, 1974; Biewener et al., 1996). When external loading was removed by detaching the calcaneal tendon, BV/TV reduced as a result of lower trabecular thickness and number (Biewener et al., 1996). Further in vivo studies have supported this. Barak et al. (2011) showed that DA and BV/TV varied predictably in the distal tibiae of sheep that loaded their ankles in different positions. Pontzer et al. (2006) also found strong correlations of DA with changes in external loading at the distal femur of guinea fowl.

However, there are several non-mechanical factors that may affect trabecular structure. It is not clear how genetic, hormonal, and environmental factors constrain its structure (Simkin et al., 1987; Judex et al., 2009; Havill et al., 2010; Devlin, 2011; Devlin and Bouxsein, 2012; Devlin et al., 2013), how its response varies based on frequency versus magnitude of mechanical loading (Skerry and Lanyon, 1995; Lambers et al., 2013), as well as anatomical region (Räth et al. 2013; Wallace et al., 2013). Furthermore, by measuring trabecular bone density throughout 9 anatomical regions in humans, Chirchir (2016) found that most sites have homogenous values, suggesting they are influenced by site-specific genetic factors. Nonetheless, computational models (Odgaard et al., 1997; Huiskes et al., 2000; Fox and Keaveny, 2001) and in vivo studies (Lanyon, 1974; Biewener et al., 1996; Pontzer et al., 2006; Barak et al., 2011) have demonstrated strong links between trabecular structure and the frequency, magnitude, and direction in which a joint is loaded.

1.2. Biomechanics of the first metatarsal

Modern humans are adapted for a bipedal mode of locomotion and possess a forefoot structure in which each metatarsophalangeal (MTP) joint acts as a weight bearing and propulsive structure during the push-off part of the stance phase (Stokes et al.,1979; Christensen and Jennings, 2009; Griffin et al., 2015). During this phase, the MTP joints dorsiflex, moving the proximal phalanges on to the dorsum of their respective metatarsal heads. This causes tightening of the plantar aponeurosis, stabilizing the foot and elevating the longitudinal arch, which changes its conformation to a stiff lever for propulsion and ultimately toe-off (Hicks, 1954; Bøjsen-Moller, 1979; Susman, 1983; Caravaggi et al. 2010; Griffin et al., 2015). As shown by in vivo studies of plantar pressure distribution within the human foot, during dorsiflexion the medial forefoot shows a spike in loading (Hutton and Dhanendran, 1981; Katoh et al., 1983; Soames, 1985; Munro, 1987; Lee and Farley, 1998; Hunt et al., 2001; Nester et al., 2007; Griffin et al., 2010a). The MT1 bears a large portion of this load and this is reflected by its large head, which experiences high compressive forces during push-off (Rodgers, 1995; Donahue and Sharkey, 1999; Vereecke et al., 2003; D'Août et al., 2004). Its external shape is also designed to stabilize the MTP joint and facilitate dorsiflexion during push-off. The superior aspect of the articular surface of the head expands to the dorsum of the bone, resulting in a raised appearance in relation to its shaft, which is thought to increase the range of dorsiflexion at the MTP joint (Stokes et al., 1979; Susman and Brain, 1988; Susman and de Ruiter, 2004; Griffin and Richmond, 2005; Griffin et al., 2010a). It is also medio-laterally wider on the dorsal aspect of the head than the plantar aspect, which has been argued to enhance joint stability during push-off and facilitate close-packing of the MTP joint (Susman and Brain, 1988; Hetherington et al., 1989; Susman and de Ruiter, 2004; Pontzer et al., 2010, Fernández et al., 2015).

Analyzing foot kinematics in extant non-human apes is less straight-forward compared to modern humans because they employ a wider range of locomotion, from terrestrial to arboreal quadrupedalism, vertical climbing, suspension, and occasional terrestrial bipedalism. However, in vivo studies of chimpanzee and bonobo footfall patterns show considerable differences from modern humans (Aerts et al., 2000; Vereecke et al., 2003; D'Août et al., 2004; Griffin et al., 2010a; Wunderlich and Ischinger, 2017). During terrestrial quadrupedal locomotion, bonobos show a higher spike in loading on the lateral aspect of the foot during push-off, with relatively little force inflicted upon the MT1 (Vereecke et al., 2003). Additionally, during vertical climbing, chimpanzees show peak loading under the medial metatarsals, when the MTP joints are plantarflexed (Wunderlich and

Ischinger, 2017). If these plantar pressure patterns can be broadly applied to non-human apes, they would suggest that the first MTP joint incurs maximum loading when it is used for grasping.

This is reflected within the shape of the MT1 head, which in all non-human apes is mediolaterally expanded on the plantar aspect (Susman, 1983; Latimer and Lovejoy, 1990; Marchi, 2005, 2010; Griffin and Richmond, 2010; Fernández et al., 2015). The same mechanism that allows for close-packing of the MTP joint during dorsiflexion in humans allows for close-packing during plantarflexion in non-human apes, increasing stability during pedal grasping (Susman, 1983; Griffin et al., 2010a). It should be noted that within non-human apes, there is variation in how the hallux is used for locomotion. Although comparative plantar pressure distribution data for Gorilla and Pongo do not exist, a substantial amount of information can be obtained through observational studies (Tuttle and Beck, 1972; Cant, 1987; Sarmiento, 1994; Remis, 1995; Gebo, 1996; Doran, 1997; Sarringhaus et al., 2014), skeletal (Susman, 1979; Shea, 1981; Inouye, 1992; Doran, 1993; Marchi, 2005; Richmond, 2007; Congdon, 2012; Drapeau and Harmon, 2013; Jashashvili et al. 2015), and soft tissue morphological analyses (Oishi et al., 2012). Such studies show different habitual positioning of the hallux; orangutans generally do not apply significant force on the hallux during suspension, whereas chimpanzees generally do (Oishi et al., 2012). Gorillas do not use their feet for suspension; when they locomote arboreally, their size restricts them to substrates of larger diameters. Their feet are used for vertical climbing or walking, but because the supports they use for climbing are usually large relative to their foot size, there is little flexion of the metatarsophalangeal and interphalangeal joints (Sarmiento, 1994; Remis, 1995).

The proximal articular surface of the MT1 is equally reflective of locomotor behavior. Within modern humans, it is relatively broad and flat, corresponding to a stable tarsometatarsal (TMT) joint complex that reduces mediolateral mobility of the hallux, and keeps it in line with the other metatarsals (Morton, 1924; Susman and Brain, 1988; Proctor et al. 2008; Proctor, 2010; Gill et al. 2015). Its broad mediolateral width is related to the bending stresses experienced near the base of the MT1, and its increased cross-sectional area is a response to high compressive forces at the joint and high tensile forces inflicted upon the ligaments (Stokes et al., 1979; Griffin and Richmond, 2005). In all other living great apes, the proximal MT1 does not experience such high loading, resulting in a proximal surface that has a smaller overall area. The TMT joint is instead adapted for a wider range of movement associated with grasping and varied locomotion. The proximal articular surface of the MT1 is concave, and the distal articular surface of the medial cuneiform is convex, allowing for multiaxial movement of the hallux that is more effective for climbing and grasping (Latimer and Lovejoy, 1990; McHenry and Jones, 2006; Tocheri et al., 2011).

1.3. Early hominin locomotion

Here, we focus specifically on Plio-Pleistocene fossil feet from South Africa, which show a diverse range of morphological features. StW 573, attributed to Australopithecus prometheus (but see Berger and Hawks, 2019), shows evidence of a slightly divergent hallux and has been interpreted as adept at tree-climbing (Clarke and Tobias, 1995; Clarke, 2013) but see (Harcourt-Smith et al., 2002). Two isolated MT1s from Sterkfontein (StW 562 and StW 595) suggest there was locomotor diversity in South African hominins. The two metatarsals are of unknown taxonomic status but were both found in Member 4, dated between 2.6 and 2.0 mya (Pickering and Kramers, 2010), and show striking differences in external morphology. StW 562 is described as more human-like based on its distal epiphysis which shows dorsal doming of the head, and because it is relatively robust. StW 595 is relatively gracile and does not show this epiphyseal feature, suggesting this individual had a more ape-like push-off mechanism (Clarke, 2013; DeSilva et al., 2019). Of particular relevance to this study are the postcranial remains of South African robust australopiths attributed to Paranthropus robustus. P. robustus is mainly represented by cranial remains (Grine, 1993; Grine and Daegling, 1993; Wood and Constantino, 2007); postcranial remains are relatively abundant, but cannot be attributed with complete confidence to the taxon. Based on pelvic, femoral, and tarsal morphology, the gait of P. robustus has been described as bipedal, but with a ‘waddling gait’ and a less efficient body weight transfer mechanism (Napier, 1964; Day and Napier, 1965; Robinson, 1972; Gebo and Schwartz, 2006). However, trabecular properties of the talus (Su and Carlson, 2017) and diaphyseal cortical bone morphology of the fifth metatarsal (Dowdeswell et al., 2017) suggest a medial weight transfer of the foot during push-off and loading of the lateral column in a human-like way.

Two complete metatarsals from Swartkrans contribute to our understanding of Early Pleistocene hominin locomotion. SKX 5017 is an isolated left MT1 recovered from the Lower Bank deposit of Swartkrans Member 1, dated to approximately 1.5-1.8 mya (Susman and Brain, 1988; Susman and de Ruiter, 2004). Along with other fossils found within this level, SKX 5017 is attributed to P. robustus. The specimen is described as short and similar in length to OH 8 and female bonobos (Susman and Brain, 1988). The base of the metatarsal has a mildly concave and ovoid shape, similar to modern great apes (Susman and Brain, 1988), although the morphology of the base and proximal shaft provide evidence that human-like plantar ligaments (and perhaps an aponeurosis) were present. Based on this basal articular morphology, and on the degree of torsion between the head and the base, there is no indication that the hallux was abducted to an ape-like degree (Susman and Brain, 1988). The head displays a mosaic of primitive and derived features. The superior articular surface of the head extends onto the dorsum of the shaft, which is an indication of increased dorsiflexion at the MTP joint. In contrast, the dorsal medio-lateral breadth of the head is narrower than the plantar breadth, suggesting the joint did not close-pack in dorsiflexion, and thus was less stable during push-off (Susman and Brain 1988).

SK 1813 is a nearly complete right MT1 found in a backfill hole of Swartkrans and is thought to have come from Member 1 or 2, but attribution to a specific stratigraphic unit or taxon cannot be made with certainty (Susman and de Ruiter, 2004). Presence of an epiphyseal line near the base signals the subadult status of this individual, with an estimated age of approximately 15 years (Susman and de Ruiter, 2004). It bears strong morphological affinities to SKX 5017, albeit the former is smaller. It has the same dorsal mediolateral narrowing on the head, and expansion of the dorsal articular surface onto the dorsum of the shaft. The base is also dorsoplantarly expanded, which is reflective of increased tensile forces from well-developed plantar ligaments in response to a bipedal gait (Susman and de Ruiter, 2004; Proctor et al. 2008; Proctor, 2010). The shape of the proximal articular surface is difficult to discern due to post-mortem damage, but is nonetheless described as concave and ovoid, typical of non-human apes (Susman and de Ruiter, 2004). In this study, we examine trabecular structure within the epiphyses of these two specimens to reconstruct aspects of their biomechanical loading regime and in doing so make inferences about the locomotor behaviours of the individuals they represent.

1.4. Previous trabecular analysis of the MT1

Predictions about how mechanical loading affects the trabecular bone within the MT1 can be made a priori based on currently-known patterns within the MT1 head of Homo sapiens, Pan troglodytes, Pan paniscus, and Gorilla gorilla (Griffin et al., 2010b). Volume of interest (VOI)-based analysis has shown that modern humans exhibit significantly higher DA values than non-human apes, consistent with a tightly constrained joint with a relatively uniaxial range of movement. The same study has shown BV/TV to be less effective at differentiating locomotor behavior between species, but this may be caused by the methodological limitations of using VOIs in analyzing trabecular structure. Overall, these results suggest that among trabecular bone properties, a high degree of anisotropy is the most indicative factor of a forefoot habitually used for propulsion during bipedal gait (Griffin et al. 2010b).

1.5. Aims and predictions

Based on known loading patterns within the forefoot of modern humans and great apes, and the mechanical adaptations of trabecular bone, we test the following hypotheses:

1. Modern humans will have a higher BV/TV within the dorsal aspect of the MT1 head and base, and non-human apes will display the opposite pattern. This corresponds to the position in which the joints close-pack and incur the highest compressive load.
2. Modern humans will show higher overall DA and non-human apes will show lower overall DA within the entire element, corresponding to the range of motion at the TMT joint and the MTP joint. We also predict that modern humans will show relatively higher DA in the dorsal regions of the epiphyses compared to the non-human apes.
3. Based on their external morphology, we hypothesize that SKX 5017 and SK 1813 will show similar trabecular distribution to modern humans. However, because of a more concave and rounded proximal articular facet in SKX 5017 indicative of a relatively mobile joint, its base will have a lower DA than modern humans.

To ensure no confounding factors relating to body size, we also test for interspecific allometry in trabecular bone variables. Following the results of previous studies on the talus and tibia of modern humans and chimpanzees (Tsegai et al., 2017), and on the lower limbs of modern humans (Saers et al.

2016), we predict that there will be no significant allometric scaling between any trabecular parameter and bone size. Furthermore, because Tsegai et al. (2017) found that the tibia and talus do not show the same patterns of scaling in regards to Tb.Th., BV/TV, or DA, we expect that the MT1 will also display allometric patterns not displayed in either element.

2. Methods

2.1. Sample

The comparative sample consists of thirty-nine MT1s from modern non-human apes and modern humans: six Pongo sp., ten Gorilla gorilla, ten Pan troglodytes, and eleven Homo sapiens. Details of the study sample are shown in **Table 1**. Orangutans were wild-shot, but their provenance is unknown, with the exception of one captive male from the Munich Zoo. Gorillas were all wild-shot in Cameroon and the French Congo. Some chimpanzee specimens were collected from the Taï National Park, Republic of Côte d'Ivoire; others were wild-shot in Cameroon. The modern human sample was composed of likely sedentary and shod individuals from two 19th-20th century cemeteries in Göttingen, Germany (for more information on the comparative sample, see SI, Table S1). Specimens were chosen if the individuals were adult, free from signs of pathology, and if their trabecular bone was well-preserved. Adult status was determined based on external morphology of the associated postcrania and dental eruption. Additional information on individual specimens is provided within the supplemental online information. Two fossil hominin MT1s were obtained from the Ditsong National Museum of Natural History and derive from the site of Swartkrans, South Africa. One is attributed to Paranthropus robustus (SKX 5017), and the other being of unassigned taxonomic status (SK 1813). SKX 5017 is complete and well-preserved, but because of extensive cortical and trabecular damage to the base of SK 1813, only the head was analyzed.

2.2. Image Acquisition

Specimens were scanned at the Max Planck Institute for Evolutionary Anthropology in Leipzig and at Cambridge University. The modern Homo and Pongo specimens were scanned using a Diondo d3 high-resolution micro-CT system in Leipzig with an acceleration voltage of 140 kV, and 120 µA and 140 µA respectively, using a 0.5 mm brass filter. The images were reconstructed as 3000 x 3000 16 bit tiff image stacks from 3240 projections with two frame averaging. The Taï Forest Pan troglodytes sample was scanned using a Skyscan 1173 with an acceleration voltage of 100 kV and 62 µA using a 1.0 mm aluminium filter. The images were reconstructed from 2240 x 2240 16 bit tiff image stacks from 2400 projections with two frame averaging. Gorilla gorilla and Pan troglodytes specimens from the Powell-Cotton Museum were scanned using a Nikon Metrology XT H 225 ST High resolution CT scanner in Cambridge University. They were scanned at an acceleration voltage of 135 kV and 135 µA with no filter. The images were reconstructed as 2000 x 2000 16 bit tiff image stacks from 1080 projections with one frame averaging. All specimens were scanned with an isometric voxel resolution between 27 and 42 µm.

2.3. Specimen segmentation

Scans were segmented into binary format using the Ray Casting Algorithm (RCA) (Scherf and Tilgner, 2009). This method is most effective where there is clear separation between bone and air, and where there is little matrix within the epiphysis. All extant taxa, along with SKX 5017 were segmented using this method. Due to a large amount of matrix within the epiphysis of SK 1813, it was segmented using a machine learning clustering algorithm that is most effective where there is matrix that falls within the greyscale range of trabecular bone (Dunmore et al., 2018). This algorithm assigns voxels in an image to one of three predefined classes, based on the probability that its greyscale value would be in each class. Therefore, it allows for segmentation of problematic areas that the RCA does not handle effectively.

2.4. Medtool

The segmented images were processed through a customized script within medtool v4.2 (www.dr-pahr.at), a python-based script manager. Each step of this method has been described by Pahr and Zysset (2009) and tested by Gross et al. (2014). Using the segmented image (**Fig. 1a**), the outer surface (**Fig. 1b**), and inner surface (**Fig. 1c**) were defined and subtracted from one another to create an image of the cortex only (**Fig. 1d**). An image of the trabecular bone (**Fig. 1e**) only was obtained by subtracting the cortex image from the original segmented image. A series of mask overlays were created to separate the cortical and trabecular bone, and ‘inside air’ from ‘outside air’ by assigning them to different grey values (**Figs. 1f, g, h**). A 3D mesh of the mask images was obtained using the computational geometry algorithms library (CGAL version 4.10, Computational Geometry, http://www.cgal.org), a mesher that creates a 3D finite element model using 3D Delauney triangulation (Delaunay, 1934). Trabecular bone was analyzed through the placement of multiple spherical VOIs onto a rectangular background grid of 2.5 mm grid spacing over the MaskSegIn image (**Fig. 1f**). VOIs were placed at each node with a set diameter of 5 mm to ensure overlap. Trabecular parameters were measured within each VOI, and values were assigned to each grid node. These values were then interpolated to the tetrahedral elements, resulting in BV/TV and DA color maps that were visualized using Paraview 3.14.1 (Sandia Corporation, Kitware. Inc).

Within each VOI, bone volume fraction (BV/TV) was calculated as the ratio of bone voxels to bone and air voxels. The trabecular orientation (second rank fabric tensor) was calculated using the Mean Intercept Length (MIL) method (Whitehouse, 1974; Odgaard, 1997). This gave results for first, second, and third eigenvectors and eigenvalues. Fabric degree of anisotropy (DA) was calculated as (1 – [eigenvalue 3/eigenvalue 1]), resulting in numbers from 0 to 1 (representing complete isotropy and anisotropy, respectively). The values within each VOI were averaged to obtain results for the entire section. In addition to BV/TV and DA, trabecular thickness (Tb.th., mm), trabecular number (Tb.N, mm^{-1}), and trabecular spacing (Tb.S, mm) were calculated within each VOI.

2.5. Statistical analysis

Because the focus of this research is on trabecular bone structure, statistical analysis was confined to the epiphyses; the shaft, which contains little to no trabeculae was separated from the head and base. In each scan, the head was separated where the articular surface on the plantar aspect terminated, as it is clearly delineated from the shaft. When viewing the element in plantar view, each metatarsal displays a pronounced curvature on the proximal and medial aspect of the shaft. The cut for the base was made where this curvature was most pronounced (**Fig. 2a)**. The base and the head were further separated into dorsal and plantar regions by taking their maximum dorso-plantar length and dividing it by half (**Fig. 2b**).

Statistical analysis was performed using RStudio v1.0.153 (RStudio Inc. 2015), and plots were generated using ggplot2 (Wickham, 2009). All trabecular variables were tested for allometry using reduced major axis regression, through the R package lmodel2 (Legendre, 2018). Because data for body size was unavailable for the study sample, the geometric mean for each specimen was used as a proxy for body size. This was calculated using five linear measurements of the metatarsal as proposed by De Groote and Humphrey (2011), which included maximum MT1 length, as well as dorsoplantar and mediolateral length of the proximal and distal articular surfaces.

Standard non-parametric tests were used because of small sample sizes, and because not all regions in all taxa showed a normal distribution. Pair-wise comparisons using Mann-Whitney U tests were conducted to investigate intraspecies differences in BV/TV and DA between the dorsal and plantar sections in the head and base. The raw dorsal and plantar BV/TV and DA values were also compared between species using Kruskal-Wallis tests to test whether the samples originate from the same distribution. Additionally, BV/TV values in both epiphyses were used to calculate the ratio of trabecular bone in the plantar versus dorsal regions. Ratios were compared between taxa using a pairwise Wilcoxon rank sum test with a Bonferroni correction. In addition to traditional non-parametric tests, differences between the BV/TV ratios of each taxon were evaluated for statistical significance using a standard resampling method (i.e., bootstrapping), which is well-suited to examine differences between means of groups with varying and small sample sizes (Efron and Tibshirani, 1993). Values from each taxon were resampled with replacement 10,000 times, from which 10,000 BV/TV ratio means were generated. Using pairwise comparison, the bootstrapped means from all taxa were randomly aligned and subtracted from means from another taxon, resulting in 10,000 differences between the means. Pairwise comparison was also used to calculate the difference between the means of the original, non-bootstrapped samples. The bootstrapped differences were then compared to the original differences. The number of times the difference between the bootstrapped means exceeded the difference between the original sample means represents a proportion that is analogous to a p-value of a one-tailed test.

Bootstrap analysis was also applied to the fossil sample to determine the likelihood that their BV/TV ratios fell within those of the extant taxa. In this case, the BV/TV ratio from the fossil was included within each extant taxon’s sample, which was then resampled and replaced. The number of times the fossil’s BV/TV ratio fell within the range of the bootstrapped mean BV/TV ratios represents the likelihood that this value would be expected within a sample from the study taxa.

3. Results

3.1. Allometry

Most trabecular parameters showed no significant allometric scaling within taxa (**Table 2**). *Gorilla* showed positive scaling of trabecular thickness and a negative scaling of trabecular number. However, while this correlation was significant for trabecular thickness ($p<0.05$), the confidence intervals of the slope contained the isometric scaling value, meaning isometry cannot be rejected. The same pattern is seen in modern humans, though none of the scaling is significant. *Pan* shows significant positive and negative allometric scaling of trabecular spacing and number, respectively. *Pongo* shows positive scaling for trabecular thickness and negative scaling for trabecular spacing. However, it shows no significant allometric scaling. In all taxa, BV/TV and DA both show a positive relationship with increased MT1 size, but without any significant positive allometric scaling. *Pan* presents a single exception, wherein BV/TV has a negative relationship with MT1 size, though it is not statistically significant. This allows for the conclusion that BV/TV and DA are not strongly linked to MT1 size (and by proxy, body size). Given the fact that BV/TV does not scale allometrically in any taxon, it can be concluded that body size, and by extension sex do not affect patterns of trabecular distribution to a significant degree.

3.2. MT1 BV/TV distribution

Figure 3 shows BV/TV distribution maps of a representative specimen from each taxon within the sample (images of the full sample are shown within the supplementary information, Figs. 1 – 4). Modern humans consistently show a greater distribution of trabecular bone within the dorsal aspect of the head. However, some individuals have higher BV/TV values closer to the centre of the epiphysis or near the cortical/trabecular boundary. BV/TV tends to be higher on the lateral side of the dorsal aspect, corresponding with the slightly valgus orientation of the phalanges in relation to the metatarsal shaft. Additionally, specimens show a consistent pattern on the plantar surface of the head wherein the trabecular bone directly below the articular surface for the sesamoid bones displays lower

BV/TV (see SI, Fig. S4). The ventral keel between the articular surfaces has generally higher BV/TV. All modern humans have higher BV/TV on the dorsal half of the MT1 base; the plantar aspect has relatively little trabecular bone, with the exception of a small area near the insertion site of the fibularis longus tendon, which is more pronounced in modern humans than in non-human apes.

All non-human apes within the sample tend to exhibit a higher concentration of trabecular bone within the plantar region of the head, with Pongo showing the most plantar concentration. Pan and Gorilla show relatively similar distributions to each other; trabecular bone has a higher concentration on the plantar aspect of the head, but it is further from the subchondral boundary than in Pongo. However, in all taxa, there is variability in the extent to which the trabecular bone extends into the centre of the distal epiphysis: some individuals have a fairly localized concentration near the subchondral bone, but others show a much deeper distribution within the entire epiphysis (e.g., see SI Figs 1-3). The pattern of trabecular bone distribution within the base is variable, but overall it is evenly distributed across the dorsal and plantar regions. Pongo shows a pattern in which the edges of the articular surface show higher BV/TV (see Fig. 2), with relatively less trabecular bone in the center of the epiphysis. In all non-human apes, the trabecular bone is distributed along an oblique plane in relation to the shaft, corresponding to the plane in which the metatarsal flexes and extends.

Figures 4 and 5 illustrate the external morphology and trabecular distribution of SKX 5017 and SK 1813, respectively. Similar to modern humans, the dorsal region of the metatarsal head of SKX 5017 exhibits a higher distribution of trabecular bone than the plantar region; although it is located more dorsally than is generally found within modern humans. This region of high BV/TV is positioned laterally and corresponds to a slightly valgus orientation of the phalanges in relation to the shaft. The remainder of the head shows an even distribution of trabecular bone, with an area of slightly higher BV/TV on the plantar aspect on the ventral keel between the articular surfaces for the sesamoid bones (this is also seen in some modern humans). The base of SKX 5017 shows high BV/TV near the dorso-medial border of the articular surface, similar to where it is seen in several non-human apes, and a slight area of high BV/TV on the plantar-lateral aspect. Both plantar and dorsal regions display high BV/TV, in contrast to modern humans which have a markedly higher and more localized trabecular bone distribution within the dorsal region.

SK 1813 (**Fig. 5**) also displays higher trabecular bone distribution within the dorsal aspect of the head, though it is more centralized within the epiphysis than in SKX 5017 or the modern human sample. Additionally, the area immediately below the cortical/trabecular boundary shows a sharp decrease in BV/TV. On the plantar aspect, where the shaft meets the head, there is another area of high BV/TV. When comparing the color map to the original CT scan, it becomes apparent that this area of high BV/TV is the result of cortical bone from the shaft extending into thick trabecular struts within the head, similar to Pan and Gorilla. However, SK 1813 shows relatively less trabecular bone within the rest of the plantar surface, resulting in a different overall distribution to all other taxa.

3.3. Regional trabecular distribution

Mean values for all trabecular parameters are shown in **Table 3,** and **Figure 6** presents box-and-whisker plots of BV/TV values among the study taxa. Within extant taxa, BV/TV tends to be highest in Pan and lowest in modern humans. Furthermore, modern humans show the highest overall DA values, and Pongo displays the lowest. It should be noted that coefficients of variation (CV) indicate that Pongo has the most variable BV/TV and DA values (with the exception of BV/TV in the modern human base). When considering overall patterns across both epiphyses, trabecular thickness is highest in Gorilla and lowest in modern humans. Trabecular number shows the opposite pattern: it is highest in modern humans and lowest in Gorilla. Trabecular spacing is highest in Gorilla; of the extant sample, it is lowest in modern humans. When considering the base and head separately, different patterns emerge between taxa. Although BV/TV is similar between the head and base, all extant non-human apes show a relatively higher number, and more tightly spaced trabeculae in the base than in the head. In all cases, BV/TV remains similar in both epiphyses as a result of thinner trabecular bone in the base. We also see a difference in DA between the head and base: despite some overlap in values, mean DA is higher in the base than in the head. In contrast, modern humans show a similar trabecular architecture in the head and in the base. Trabecular number is slightly higher in the head, resulting in higher BV/TV, but to a lesser extent than the non-human apes.

The two fossils show a different trabecular bone structure from each other, as well as to the comparative sample. SKX 5017 exhibits the highest overall BV/TV of all taxa as a result of a relatively higher number of thicker and closely spaced trabeculae. Similar to the non-human apes, it has a relatively higher number, and more closely spaced trabeculae in the base than in the head. SK 1813 shows a BV/TV value that falls well within the range of the African great apes. Its trabecular number is higher, and its trabecular spacing is lower than all other taxa. Its trabecular thickness falls within the range of all taxa. Both fossils have closely spaced trabeculae, but compared to SKX 5017, SK 1813 has a higher number of thinner trabeculae. Disregarding their absolutely thicker trabeculae than modern humans, the MT1 heads of the fossil specimens have an overall higher number of closely spaced trabeculae, a pattern seen in the head of modern humans; SKX 5017 shows values in the base within the range of non-human apes.

Regional summary statistics for all analyzed trabecular parameters can be seen in the SOM (SOM Table S1). Mann-Whitney U tests reveal significant differences in mean BV/TV values between the dorsal and plantar regions of the MT1 heads of all studied taxa (Fig. 6). Non-human apes show a higher BV/TV within the plantar region, whereas modern humans have higher BV/TV in the dorsal region. Within the base of the MT1, only modern humans show significant differences in BV/TV between the dorsal and plantar regions, with relatively higher values in the dorsal region. SKX 5017 shows higher BV/TV in the dorsal regions of the head and base, similar to modern humans, but with overall higher BV/TV. The SK 1813 head displays overall higher BV/TV in the dorsal region as well, though it has absolutely lower BV/TV than SKX 5017.

Figure 7 presents ratios of dorsal-to-plantar BV/TV within the heads and bases of all taxa. Within all non-human apes, the base of the metatarsal shows a BV/TV ratio approximating a value of one, indicating relatively equal BV/TV between the dorsal and plantar regions. In contrast, modern humans display a much higher ratio, indicating relatively higher BV/TV within the dorsal section of the base. Within the head, all extant non-human apes show a ratio below one, indicating relatively higher BV/TV within the plantar region, whereas modern humans retain a higher proportion of trabecular bone within the dorsal region. Results from post-hoc pairwise Wilcoxon rank sum tests from the head reveal significant differences between the BV/TV ratio of modern humans and all extant non-human apes ($p<0.0005$), and between Gorilla and Pongo ($p<0.01$) (**Table 4**). No statistically significant differences were found between Pongo and Pan, or between Gorilla and Pan.

Within the base, no statistically significant differences were found in BV/TV ratio between the non-human apes, but all showed significant differences from modern humans (p<0.0005). Bootstrap analyses support these results, showing a similar distribution of trabecular bone within the base of all non-human apes (see SI Fig. S6).

Results from bootstrap analyses of BV/TV ratio means in the base reveal significant differences between the BV/TV ratio of SKX 5017 and all extant taxa, with a value lower than modern humans (p<0.01), and higher than Pongo (p<0.01), Gorilla (p<0.01), and Pan (p<0.01) (**Fig. 8**). Bootstrap analyses from the head show that the BV/TV ratio of SKX 5017 falls within the range of modern humans (p>0.05), and that the BV/TV ratio of SK 1813 falls outside the range of all extant taxa (p<0.01). The distribution, though more dorsal than plantar, falls below the range seen in modern humans, and above the range seen Pongo, Gorilla, and Pan (**Fig. 9**).

Differences in DA values between taxa are illustrated in **Figure 10**. All taxa show significant differences between DA in the plantar and dorsal regions, with modern humans showing the absolute highest values, and Pongo the lowest. Results from the Kruskal-Wallis post hoc test for differences in DA show that modern humans have significantly higher DA in the head than all taxa, and significantly higher DA in the base than Pongo and Gorilla. Among the non-human apes, only Pan and Pongo differ significantly in the head. In the base, Pan is the only significantly different taxon, with the highest mean DA value (**Table 5**). There is no statistically significant interspecies difference in the ratio of DA between the dorsal and plantar regions. All modern taxa display a pattern where the dorsal sections of both epiphyses possess similar DA values that are significantly higher than the values seen in the plantar sections. Like the modern taxa, SKX 5017 displays higher DA in the dorsal regions, however, DA in the dorsal region of the base is absolutely higher than DA in the dorsal region of the head, and DA in the plantar region of the base is absolutely higher than the plantar region of the head. The plantar region of the base and the dorsal region of the head share close values, a pattern not seen in the entire extant sample. SK 1813 displays a similar DA pattern to the extant taxa, with higher values in the dorsal region than in the plantar region, although it has the absolute lowest values.

Figures 11 and **12** display bivariate plots of BV/TV and DA values from the head and base, respectively. Modern humans possess lower BV/TV and higher DA, distinguishing them from other taxa. Within the non-human apes, *Pan* shows overall higher DA, followed by *Gorilla* and *Pongo*, respectively, but their BV/TV values overlap. As mentioned earlier, *Pongo* shows the widest range of BV/TV values. BV/TV values in both SKX 5017 and SK1813 are well above those in modern humans, and within the range of the non-human apes**.** DA values are lower in SK 1813 and SKX 5017 than in modern humans, though they are absolutely lowest in the former, within the range of *Pongo*.

4. Discussion

4.1. Effect of body size on trabecular bone structure

Most trabecular parameters do not to scale allometrically within species. Like other studies (Doube et al., 2011; Ryan and Shaw, 2013), results from this analysis show a positive, but isometric relationship between BV/TV and body size. The only taxon to show positive scaling of trabecular thickness is *Gorilla*, supporting previous findings (Doube et al., 2011). However, because the confidence intervals of the slope contain the isometric scaling value, an isometric relationship cannot be rejected. All other taxa show no allometric scaling of trabecular thickness (see also Mullender et al., 1996; Swartz et al., 1998). In *Pan*, trabecular spacing shows positive allometric scaling and trabecular number shows negative allometric scaling. These results contradict previous studies of trabecular allometry in primates (mainly in the femur and humerus), which emphasize negative allometric scaling of trabecular spacing and thickness (Ryan and Ketcham, 2002, 2005; Fajardo et al., 2007; Ryan and Walker, 2010; Ryan and Shaw, 2012). This could be the result of smaller sample sizes used in this study, or because this study observes interspecies allometry. Our results are partially consistent with a previous study on allometry between *Pan* and Homo (Tsegai et al., 2017). Certain trabecular variables of the MT1 show similar scaling patterns as the talus, but others are more consistent with the distal tibia. Overall, these results suggest that scaling within species as a result of individual size variation and sexual dimorphism do not play an important role in trabecular structure, and that different elements throughout the skeleton may show variable allometric scaling patterns.

4.2. Trabecular distribution in extant taxa

Within the extant sample, the trabecular parameters that most effectively separate each locomotor mode are relative BV/TV and absolute DA. Trabecular bone acts as structural support during joint loading, meaning higher BV/TV should be located in the area of the epiphysis where the joint incurs high compressive loading (Rubin et al., 2002; Barak et al., 2011). A higher distribution of trabecular bone in the plantar region offers support for loading during plantarflexion, and a higher distribution in the dorsal region offers support for loading during dorsiflexion. The first hypothesis is that modern humans show higher BV/TV within the dorsal aspect of the epiphyses. This is supported here based on significantly higher BV/TV ratio in the MT1 of modern humans than all other extant taxa, which corresponds to its higher range of dorsal excursion, and to the position in which the MTP joint incurs maximum loading (Rodgers, 1995; Donahue and Sharkey, 1999; Vereecke et al., 2003; D'Août et al., 2004). Furthermore, the tarsometatarsal joint, which is more limited in mobility than the MTP joint, is stable and experiences movement along a single plane (Morton, 1924; Susman and Brain, 1988; Proctor et al. 2008; Gill et al. 2015). Therefore, it exhibits a tightly constrained pattern within the base of the MT1.

Within the head, non-human apes show a plantar distribution of trabecular bone associated with high compressive loading during plantarflexion. This corresponds to studies of plantar pressure distribution in Pan troglodytes (Wunderlich and Ischinger, 2017), which show that the MTP joint incurs peak plantar pressure during vertical climbing, when it is plantarflexed. Plantar pressure data on Pongo during suspensory locomotion is entirely absent, making inferences about loading at its MTP joint speculative. However, results from this study suggest that it was nonetheless loaded higher in plantarflexion than dorsiflexion. Although the Pongo hallux is less capable of force gripping compared to Gorilla and Pan, its actual use during suspensory locomotion may not be as limited as previously thought. Commonly held ideas emphasize that Pongo show reduced hallucal recruitment during suspensory locomotion (Morton, 1924; Midlo, 1934; Tuttle and Rogers, 1966; Tuttle, 1969; Marchi, 2010), however, there is evidence that its true use is somewhat underreported (McClure et al., 2012).

The great apes, which have a more mobile tarsometatarsal joint, show evenly distributed BV/TV within the entire base. This could be reflective of the variable ways in which these taxa load the forefoot, resulting in a generalized trabecular structure adapted for a wide range of motion and loading. Despite similar BV/TV ratios, color maps show differences in the distribution of trabecular bone within the base of Pongo, Gorilla, and Pan. As mentioned earlier, trabecular bone within the Pongo base shows a higher distribution near the edges of the articular surface, whereas Gorilla and Pan show a relatively higher distribution throughout the entire epiphysis. This could be related to locomotor differences between the taxa. Pongo employs a hook-like grip during suspension without applying significant force on its hallux, contrary to Pan and Gorilla, which both use the hallux more forcefully (Sarmiento, 1994; Remis, 1995; Oishi et al., 2012). The low compressive and tensile forces experienced by the Pongo MT1 base might explain why the trabecular bone does not extend as far into the centre of the epiphysis. This could mean that BV/TV ratio is better at differentiating broad locomotor patterns (i.e., between bipedalism and vertical climbing), whereas BV/TV color maps may better capture subtle differences in joint positioning and loading between types of terrestrial quadrupedalism or arboreal locomotion.

Griffin et al. (2010b) analyzed the trabecular structure within the MT1 head of Pongo, Gorilla, Pan, and Homo. By placing three VOIs in the epiphyses, they found that all taxa showed higher BV/TV in the dorsal region of the head. Based on these results, they concluded that BV/TV was not useful in differentiating habitual joint positioning. Results from this study contradict these results. Though BV/TV ratio is not useful in differentiating locomotion between non-human apes, it separates bipedalism from all other forms of locomotion. The reason for these conflicting results could be methodological. Although overall, non-human apes show higher BV/TV in the plantar region of the head, there is variation in where within the epiphysis BV/TV is highest. Some specimens show higher trabecular distribution near the subchondral bone, and others show higher distribution deeper within the epiphysis (and our results indicate that concentrations are not always in the midline of the joint). Thus, VOIs restricted to only a portion of the epiphysis capture only a subset of the variation compared to a whole-epiphysis approach.

It is also worth noting that BV/TV ratio is likely better at differentiating between broad locomotor modes because absolute BV/TV does not necessarily reflect the magnitude of load applied to an element. Modern humans show systematically lower BV/TV than all other taxa, despite their medial forefoot experiencing higher loading during push-off than non-human apes (Vereecke et al., 2003). Lower overall BV/TV has been previously observed in other studies of cortical and trabecular bone in modern humans (Lieberman, 1996; Chirchir et al., 2015; Saers et al., 2016; Tsegai et al., 2017) and has been suggested to be linked to higher sedentism in relation to early hominins and recent hunter-gatherers. Because the sample represented in this study is of likely shod and sedentary modern humans, it is also worth noting that the low overall BV/TV values seen here may not reflect the entire range of human variation (Shaw and Stock, 2009a, b; 2013; Ryan and Shaw, 2015; Saers et al., 2016). For this reason, in this study, BV/TV is mainly relevant when its relative distribution is analyzed. Further studies including shod and unshod populations, as well as hunter-gatherers may contribute to our understanding of overall BV/TV within modern humans.

The second hypothesis is that modern humans show higher DA within the MT1 than all non-human apes, and that this is most apparent in the dorsal regions. This is partially supported; modern humans show overall higher DA than Gorilla and Pongo throughout both epiphyses, but they do not differ significantly from Pan in the base. Nevertheless, higher overall DA within modern humans corresponds with the hypothesis that a more uniaxial range of movement will result in stereotypically oriented trabeculae. Similar to Griffin et al. (2010b), we found that all taxa show higher DA dorsally, suggesting that non-biomechanic factors may influence this trabecular variable. As such, caution should be applied when inferring locomotor behavior based on DA alone. Within non-human apes, DA values overlap, meaning the modes of locomotion employed by these taxa cannot be as clearly differentiated using DA. For example, given the fact that Gorilla is considered the most terrestrial taxon, it is noteworthy that it is most similar in DA to Pongo, the most arboreal taxon. This may also be explained by different factors; Gorilla may simply load its hallux in variable positions, or the individuals in this sample may have been relatively arboreal. There is evidence that western lowland gorillas display considerable arboreal behavior, with females spending more time on terminal branches at frequencies similar to Pan (Remis, 1995, 1999). Because the gorillas in this study are all western lowland, there is the possibility that they were also relatively arboreal. Ultimately, there may be substantial overlap in degree of arboreality between non-human apes, making DA fairly weak in differentiating their locomotor modes. These results simply demonstrate that modern humans have the least variable MT1 positioning. In order to associate DA with a specific mode of locomotion, it may be more informative to look at directionality of trabeculae as opposed to overall DA or DA ratio. DA is a measure of how similarly aligned trabeculae are in relation to each other, but does not provide information on which axis the trabeculae are aligned in. Because trabeculae orient themselves along the principal axis of movement, the actual direction in which they are aligned might be more informative in reconstructing movement in a joint (Biewener et al., 1996; Ryan and Ketcham, 2002; Pontzer et al., 2006; Saparin et al., 2011). Future analyses could map, in the same manner as absolute values of trabecular variables, regional differences in primary trabecular orientation throughout the epiphysis.

Similarities in trabecular patterning between non-human apes are emphasized when plotting DA against BV/TV. The head shows considerable overlap in values; Gorilla overlaps with Pongo and Pan in both variables. Combined, modern humans do not show overlap in DA and BV/TV with the other taxa, but their values are close. This could be due to the fact that the range of motion at the MT1 head is limited to flexion and extension, meaning all taxa show a similar range of movement here. DA in the base distinguishes taxa better; this could be because the TMT joint may better reflect differences in hallucal positioning. The problem with this explanation is that modern humans and Pan show similar DA in base, despite known differences in joint loading and positioning at the TMT joint. Perhaps Pan loads this joint along a relatively constrained axis, although further observational and biomechanical analyses would have to be performed to test this. It is also worth noting that non-human apes show overall higher DA in the base than the head, whereas modern humans show similar values in both epiphyses. This could be reflective of the fact that the former load their proximal and distal MT1 joints in variable positions, contrary to relatively constrained modern human MT1.

Despite broad similarities in BV/TV and DA between non-human apes, differences can be observed between them when comparing other trabecular parameters (Tb.Th., Tb.Sp., Tb.N.). Gorilla displays relatively few, thick, and widely spaced trabeculae, whereas Pongo is characterized by relatively more, thinner, and closely spaced trabeculae. Pan shows values intermediate between Pongo and Gorilla. Of the non-human apes, the overall pattern in Pongo is most similar to modern humans, which have the thinnest trabeculae, but are similar in number and spacing. However, these differences in trabecular properties among species may not be significantly different and small sample sizes may not reflect overall patterns within species; furthermore, the functional implication of these differences, if any, is unknown.

4.3. SKX 5017 and SK 1813

The original descriptions of SKX 5017 and SK 1813 (Susman and Brain, 1988; Susman and de Ruiter, 2004) suggest that both have a combination of primitive and derived features, and that based on multivariate analyses of various linear measurements, both were most similar to modern humans. Additional multivariate analysis has suggested a unique mode of locomotion in both specimens characterized by relatively facultative bipedalism (Zipfel and Kidd, 2006). Research on the proximal articular surface of both specimens has differentiated them from modern humans (Proctor et al., 2010) and from one another (Vernon, 2013). Proctor et al. (2010) measured the curvature of the surface using 3D geometric morphometric analysis, and found that SK 1813 did not group with modern humans but showed affinities to SKX 5017. Based on an 'ape-like' curvature, both were interpreted as belonging to Paranthropus. Another analysis groups SKX 5017 with Pan and western gorillas in terms of mediolateral articular surface curvature, and SK 1813 with modern humans and Papio (Vernon, 2013). Based on these conflicting results, it is difficult to determine how 'human-like' or 'ape-like' the proximal articular surface is, and even less so the locomotor behavior associated with this shape.

The third hypothesis is that the two fossils will show similar trabecular distribution to modern humans, but that the base of SKX 5017 will show lower DA than in modern humans due to its relatively concave proximal articular facet. This is partially supported: based on its BV/TV ratio, SKX 5017 shows a similar trabecular distribution to modern humans in the head, but its base displays a more even dorso-plantar trabecular distribution. As predicted, DA within the base of SKX 5017 is lower than in modern humans. Similar to modern humans and SKX 5017, the SK 1813 head shows a BV/TV ratio over one, indicating a dorsal distribution of trabecular bone. However, the ratio is significantly lower than in modern humans; in fact, it falls outside the range of all taxa within the comparative sample. Based on the color maps, SKX 5017 shows evidence of an MTP joint that was loaded in hyper-dorsiflexion. The external morphology of the head, specifically its raised superior aspect in relation to the dorsum of the shaft, indicates it was capable of a wide range of dorsiflexion at the MTP joint (Susman and Brain, 1988). However, because of its dorsal mediolaterally narrow width, previous analyses have not reached a consensus on how the joint was loaded. It has been suggested that this combination of features prevented close-packing in dorsiflexion at the MTP joint, and resulted in instability during bipedal locomotion (Susman and Brain, 1988; Susman and de Ruiter, 2004). Though bootstrap analysis places SKX 5017 BV/TV ratio well within the range of modern humans, the color maps suggest the element was not loaded in the same way. SKX 5017 shows a hyper-dorsal distribution of bone not seen in modern humans. Because this is not seen in any of the comparative taxa, it cannot be linked with confidence to a specific type of locomotion. This may fit in with previous suggestions that the joint was less stable during dorsiflexion: because the joint did not close-pack in dorsiflexion it hyper-extended, resulting in a more dorsal trabecular distribution. When taking into account other trabecular parameters (i.e., DA), it could imply a form of locomotion not seen in modern taxa. For example, this concentration of trabecular bone could be caused by habitual hyper-dorsiflexion at the MTP joint from foot placement that is directly against a vertical substrate. This has been noted to occur in arboreal contexts in modern human populations that collect resources from trees and is directly associated with extreme dorsiflexion of the ankle and forefoot (Kraft et al., 2014). Research on midfoot flexibility in modern humans has also shown that lateral midfoot plantar pressure is strongly correlated to the magnitude of midfoot flexion, and that individuals with higher lateral midfoot plantar pressure tend to have increased dorsiflexion at the hallucal MTP joint (Bates et al., 2013; DeSilva and Gill, 2013; DeSilva et al., 2015). How the trabecular bone in the MT1 of such individuals is structured is not known. However, this suggests that hyper-dorsiflexion at the MTP joint of SKX 5017 could be the result of a fairly mobile midfoot lacking a human-like arch.

The trabecular structure of the base of the SKX 5017 MT1 combined with its external morphology emphasize a different loading pattern from modern humans. Susman and Brain (1988) described the hallux as adducted based on their description of the base as relatively flat and superoinferiorly orientated. However, geometric morphometric analyses have shown that it shares morphological affinities to Gorilla, including a relatively oblique curvature and a concave surface, albeit to a lesser extent (Proctor et al., 2008). Ultimately, because we don’t have a complete P.

robustus foot, it is difficult to tell with certainty whether it was abducent or adducted. However, results here show that the base does not adhere to a completely modern human-like trabecular structure. Though SKX 5017 has a higher ratio of trabecular bone within the dorsal aspect, there is relatively more trabecular bone within the plantar region than is observed in modern humans. As a result, the BV/TV ratio within the base of SKX 5017 is lower than in modern humans, but higher than is observed in all other non-human apes. The higher BV/TV ratio in the head suggests the element was loaded in dorsiflexion. However, the relatively lower ratio in the base suggests it could have still been loaded in plantarflexion. Combined with the fact that the proximal articular surface is concave compared to modern humans, this could be reflective of a TMT joint that has retained adaptations for grasping. DA within the base also suggests the TMT joint was more mobile than in modern humans: it is within the range of Gorilla, Pan, and Pongo, and like these taxa, is higher within the base than the head. This implies that the two epiphyses were capable of differential movement, and that unlike in modern humans, the element was not tightly constrained at both joints.

Additional trabecular parameters emphasize the unique nature of its trabecular structure. Though its trabecular thickness is within the range of modern great apes, SKX 5017 shows a structure in the head characterized by a high number of closely spaced trabeculae, which is seen in the head of modern human MT1s. Trabecular parameters within the base fall within the range of modern non-human apes. The functional implication of this is not certain, but it emphasizes the unique trabecular structure of SKX 5017: it is more ‘human-like’ in the head, and more ‘ape-like’ in the base.

It is worth noting that there is a prominent osteophyte on the dorsal aspect of the shaft, proximal to the articular surface of the head. This could be the result of a traumatic injury sustained in life, or a condition called hallux rigidus, which produces exostoses on the head of the first metatarsal (Susman and Brain, 1988). However, this condition is accompanied with flexed interphalangeal joints, which conflicts with the distribution of trabecular bone in the metatarsal head that indicates a dorsiflexed rather than plantarflexed MTP joint.

Similar to modern humans and SKX 5017, SK 1813 shows a more dorsal trabecular distribution in the head, which is reflective of a joint that was habitually loaded in dorsiflexion. It has been described by Susman and de Ruiter (2004) as similar in morphology and function to SKX 5017;

both metatarsals have a short, strait shaft, and medio-laterally narrow dorsal aspect of the head. However, the trabecular structure reveals considerable differences between the two specimens. SK 1813 displays BV/TV that is absolutely lower than SKX 5017, within the range of Pongo, Gorilla, and Pan, and a lower DA, closer to the range of Pongo. The distribution of trabecular bone, though more dorsal than plantar, falls equally between the ranges of non-human apes and modern humans, meaning it does not conform to any modern pattern. It is difficult to interpret joint positioning of SK 1813 accurately because only the head was analyzed, and because it is a subadult. Though modern humans retain a relatively consistent locomotor mode throughout ontogeny (Sutherland et al., 1980; Beck et al., 1981; Raichlen et al., 2015: but see Zeininger et al., 2018), juvenile and subadult gorillas, chimpanzees, and bonobos display much more arboreal behavior than adults (Doran, 1997; Sarringhaus et al., 2014). Trabecular structure is known to change throughout ontogeny (Ryan and Krovitz, 2006; Gosman and Ketcham, 2009; Raichlen et al., 2015; Saers, 2017) especially in regards to DA (Gosman and Ketcham, 2009; Abel and Macho, 2011). Because its taxonomic affiliation and life history are uncertain, it is not known whether its locomotor repertoire was as variable throughout ontogeny as modern apes, or as constrained as modern humans. It is possible that this hominin would have loaded its hallux in variable positions based on its lower BV/TV ratio than modern humans, and that it experienced multiaxial loading based on its low DA.

Additionally, SK 1813 displays the absolute highest trabecular number and the lowest trabecular spacing, which is a pattern seen in modern humans and SKX 5017. The taxonomic affiliations of both specimens are currently uncertain; analyses of the external morphology have provided contradictory opinions (Susman and Brain, 1988; Susman and de Ruiter, 2004; Proctor et al., 2010; Vernon, 2013). Here, we have shown that the BV/TV ratios between the two fossils are considerably different, implying different types of MTP joint loading. However, all other trabecular parameters represent a normal range of variation when compared to the intraspecies variation in other living taxa. Based on these results, we can only suggest that these hominins incurred different joint loading during locomotion.

4.4. Interpretation of Paranthropus locomotion

Debates about australopith and Paranthropus locomotion have emphasized different types of locomotion based on conflicting morphological evidence that shows derived features adapted for bipedalism, and primitive features indicative of climbing and pedal grasping (Stern and Susman, 1983; Susman et al., 1984; Susman and Brain, 1988; Grine and Susman, 1991; Susman and de Ruiter, 2004). Research on P. robustus locomotion is fairly limited because postcranial fossils are scarce and often not securely attributed to the taxon. Its postcranial morphology is described as gracile and of small stature (McHenry, 1991), and its locomotion has been described as bipedal with a 'less efficient' gait compared to modern humans (Napier, 1964; Robinson, 1972). Additionally, its radial morphology has been suggested to indicate retained arboreal abilities (Grine and Susman, 1991). Recently, the locomotor behavior of . boisei has been characterized by combined terrestrial bipedalism and occasional arboreality based on scapular, radial, humeral, femoral, and tibial morphology (Dominguez-Rodrigo et al., 2013; Green et al., 2018). If Paranthropus represents a monophyletic group, it is possible that P. robustus would have had similar postcranial morphology to P. boisei. However, the efficacy of using postcranial elements in determining phylogenetic association is uncertain; additionally, despite potentially monophyletic status, postcranial morphology between the two species could vary based on differing ecological niches.

Recently, research on P. robustus pedal elements (TM 1517) has supported the idea of an overall bipedally adapted foot. Trabecular structure in the talus has been shown to display increased DA in parts of the element associated with a medial weight shift during the stance phase, and by extension a human-like bipedal gait (Su and Carlson, 2017). Nonetheless, interpretations are still uncertain: higher BV/TV in the lateral region was suggested to indicate a degree of lateral loading intermediate in magnitude between modern human and anthropoid tali. However, diaphyseal cross-sectional properties of an MT5 from Swartkrans (SKX 33380) suggest human-like loading in the lateral column of the foot (Dowdeswell et al., 2017). Although, as with other Swartkrans postcranial elements, it should be noted that this MT5 is not linked to P. robustus with absolute certainty. Cumulatively, analyses of Paranthropus locomotion based on trabecular structure and external morphology show features that suggest habitual bipedalism, with an indication that the overall structure of the foot was more mobile, allowing for multiaxial movement at the MTP and TMT joints

(Napier, 1964; Robinson, 1972; Susman and Brain, 1988; Susman and de Ruiter, 2004; Dominguez-Rodrigo et al., 2013; Dowdeswell et al., 2017; Su and Carlson, 2017).

Based on patterns of BV/TV and DA within the metatarsal, there is evidence that the Paranthropus foot (associated with SKX 5017) possessed a habitually dorsiflexing MTP joint that was capable of a relatively multiaxial range of movement. The taxonomic status of SKX 5017 is reasonably-well established, as the layer in which it was found (Member 1) is represented by more than 95% Paranthropus remains (Susman and Brain, 1988). We do not know exactly how its external morphology compares to early Homo MT1s, meaning we cannot rule out the possibility that this element belongs to early Homo. Susman and Brain (1988) have emphasized its morphological similarities with OH 8, and others have noted that the SKX 5017 base is more similar to A. afarensis (A.L. 333-54), suggesting it belongs to a different taxon than early Homo (Proctor, 2008; Vernon, 2013). However, either possibility is uncertain since we do not know the definite taxonomic status of OH 8 (DeSilva et al., 2010). Therefore, these interpretations can only be applied to P. robustus with reasonable certainty. It is not certain whether SK 1813 represents P. robustus as well, but the trabecular structure of the two fossil specimens is different in BV/TV ratio and DA, indicating different habitual joint loading. However, we refrain from making taxonomic attributions to SK 1813 based on trabecular structure alone. If the trabecular pattern preserved here represents its adult structure, it could indicate two different species (P. robustus and Homo sp.), but enough is not known about Paranthropus and early Homo postcranial variability to make that claim. Furthermore, if the trabecular structure seen in SK 1813 reflects a subadult mode of locomotion that differs from adult locomotion, it may very well represent the same species as SKX 5017 at an earlier ontogenetic stage.

5. Conclusions

Studies of trabecular bone structure have provided mixed results in its utility in inferring habitual joint positioning (Ryan and Ketcham, 2002; Fajardo et al., 2007; DeSilva and Devlin, 2012). However, it is possible that elements in closer contact to the substrate may be more reflective of locomotor behavior because they directly absorb compressive loads associated with ground reaction forces (Maga et al., 2006; Kivell, 2016). The MT1 shows particular promise because it is a relatively simple element with adjacent joints that show a consistent range of motion. Results from this study strengthen its application in inferring fossil hominin locomotion by providing evidence that its trabecular structure can be linked to habitual joint positioning and loading of the forefoot within an extant ape sample. The most apparent differences are seen between modern humans and all other non-human apes, indicating that the relatively constrained and stable structure of the human foot results in specific trabecular patterning. BV/TV reflects the position in which the joint experiences the highest load, and DA reflects its range of motion. Though these parameters do not statistically differentiate variation in non-human ape locomotion, obligate bipedalism presents clear signals. Human bipedal locomotion is reflected in the dorsally distributed and anisotropic trabecular bone structure in the MT1, while the more arboreally adapted non-human MT1 exhibits more plantarly distributed, and relatively less anisotropic trabecular bone. This study also highlights the importance of trabecular bone analysis in the context of paleoanthropology. The two fossil specimens, which have been described as highly similar in external morphology, present different trabecular bone structures that would imply variable modes of locomotion. We find that the MTP joint was loaded differently in the two specimens: one in hyper-dorsiflexion, and the other in a manner intermediate between modern humans and non-human apes. Whether this is due to ontogenetic or phylogenetic factors is unknown. Ultimately, we show that trabecular bone structure can be associated with known modes of locomotion in modern taxa, and that it can be informative in in reconstructions of fossil hominin behavior.

Acknowledgements

For access to specimens, we thank the Max Planck Institute for Evolutionary Anthropology (Christoph Boesch and Jean-Jacques Hublin), the Powell-Cotton Museum (Inbal Livine), the Johann-Freidrich-Blumenbach-Institutfür Zoologie und Anthropologie der Georg-August-Universität Göttingen (Birgit Großkopf), and the Zoologische Staatsammlung Munich (Anneke van Heteren). For scanning, we thank David Plotzki (Max Plank Institute for Evolutionary Anthropology) and Keturah Smith (Cambridge University). For comments on previous versions of this manuscript we thank Leoni Georgiou.

Funding: This research was supported by the Max Planck Society (MMS) and the European Research Council Starting Grant #336301 (MMS) and the University of Kent (KK and MMS).

References

Abel, R., Macho, G.A., 2011. Ontogenetic changes in the internal and external morphology of the ilium in modern humans. American Journal of Anatomy 218, 324-335.

Aerts, P., Van Damme, R., Van Elsacker, L., Duchêne, V., 2000. Spatio-temporal gait characteristics of the hind-limb cycles during voluntary bipedal and quadrupedal walking in bonobos (Pan paniscus). American Journal of Physical Anthropology 111, 503-517.

Barak, M.M., Lieberman, D.E., Hublin, J.-J., 2011. A Wolff in sheep's clothing: Trabecular bone adaptation in response to changes in joint loading orientation. Bone 49, 1141-1151.

Barak, M.M., Lieberman, D.E., Hublin, J.-J., 2013. Of mice, rats and men: Trabecular bone architecture in mammals scales to body mass with negative allometry. Journal of Structural Biology 183, 123-131.

Bates, K.T., Collins, D., Savage, R., McClymont, J., Webster, E., Pataky, T.C., D'Août, K., Sellers, W.I., Bennett, M.R., Crompton, R.H., 2013. The evolution of compliance in the human lateral mid-foot. Proceedings of the Royal Society B 280, 20131818.

Beck, R.J., Andriacchi, T.P., Kuo, K.N., Fermier, R.W., Galante, J.O., 1981. Changes in the gait patterns of growing children. Journal of Bone Joint Surgery 63, 1452-1457.

Berillon, G., 1999. Geometric pattern of the hominoid hallucal tarsometatarsal complex. Quantifying the degree of hallux abduction in early hominids. Comptes Rendus de l'Académie des Sciences IIA 328, 627-633.

Berger, L.R. and Hawks, J., 2019. Australopithecus prometheus is a nomen nudum. American Journal of Physical Anthropology 168, 383-387.

Bertram, J., Swartz, S., 1991. The law of bone transformation - A case of crying Wolff. Biological reviews of the Cambridge Philosophical Society 66, 245-273.

Biewener, A., Fazzalari, N., Konieczynski, D., Baudinette, R., 1996. Adaptive changes in trabecular architecture in relation to functional strain patterns and disuse. Bone 19, 1-8.

Bøjsen-Moller, F., 1979. Calcaneocuboid joint and stability of the longitudinal arch of the foot at high and low gear push off. Journal of Anatomy 129, 165-176.

Cant, J.G.H., 1987. Positional behavior of female bornean orangutans (Pongo pygmaeus). American Journal of Primatology 12, 71-90.

Caravaggi, P., Pataky, T., Günther, M., Savage, R., Crompton, R., 2010. Dynamics of longitudinal arch support in relation to walking speed: Contribution of the plantar aponeurosis. Journal of Anatomy 217, 254-261.

Carlson, K.J. 2005. Investigating the form-function interface in African apes: Relationships between principal moments of area and positional behaviors in femoral and humeral diaphyses. American Journal of Physical Anthropology 127, 312-334.

Carlson, K.J., Lublinsky, S., Judex, S., 2008. Do different locomotor modes during growth modulate trabecular architecture in the murine hind limb? Integrative and Comparative Biology 48, 385-393.

Chang, G., Pakin, S.K., Schweitzer, M.E., Saha, P.K., Regatte, R.R., 2008. Adaptations in trabecular bone microarchitecture in Olympic athletes determined by 7T MRI. Journal of Magnetic Resonance Imaging: An Official Journal of the International Society for Magnetic Resonance in Medicine 27, 1089-1095.

Chirchir, H., 2016. Limited trabecular bone density heterogeneity in the human skeleton. Anatomy Research International 2016, 7.

Chirchir, H., Kivell, T.L., Ruff, C.B., Hublin, J.-J., Carlson, K.J., Zipfel, B., Richmond, B.G., 2015. Recent origin of low trabecular bone density in modern humans. Proceedings of the National Academy of Science 112, 366-371.

Christensen, J.C., Jennings, M.M., 2009. Normal and abnormal function of the first ray. Clinics in Podiatric Medicine and Surgery 26, 355-371.

Clarke, R.J., Tobias, P.V., 1995. Sterkfontein Member 2 foot bones of the oldest South African hominid. Science 269, 521-524.

Clarke, R.J., 2013. *Australopithecus* from Sterkfontein Caves, South Africa. In: Reed, K.E., Fleagle, J.G., Leakey, R.E. (Eds.), The Paleobiology of *Australopithecus*. Springer, New York, pp. 105-124.

Congdon, K. 2012. Interspecific and ontogenetic variation in proximal pedal phalangeal curvature of great apes (Gorilla gorilla, Pan troglodytes, and Pongo pygmaeus). International Journal of Primatology 33, 418-427.

Cowin, S., Hart, R., Balser, J., Kohn, D., 1985. Functional adaptation in long bones - establishing in vivo values for surface remodeling rate coefficients. Journal of Biomechanics 18, 665-&.

D'Août, K., Vereecke, E., Schoonaert, K., De Clercq, D., Van Elsacker, L., Aerts, P., 2004. Locomotion in bonobos (Pan paniscus): Differences and similarities between bipedal and quadrupedal terrestrial walking, and a comparison with other locomotor modes. Journal of Anatomy 204 353-361.

Day, M.H., Napier, J.R. 1965. Fossil foot bones. Current Anthropology 6, 419-420.

De Groote, I., Humphrey, L.T., 2011. Body mass and stature estimation based on the first metatarsal in humans. American Journal of Physical Anthropology 144, 625-632.

Delaunay, B., 1934. Sur la sphère vide. À la mémoire de Georges Voronoï. Izvestiya Akademiya Nauk SSR, Seriya Geologicheskaya 793-800.

DeSilva, J.M., Zipfel, B., Van Arsdale, A.P., Tocheri, M.W., 2010. The Olduvai Hominid 8 foot: adult or subadult? Journal of Human Evolution 5, 418-423.

DeSilva, J.M., Devlin, M.J., 2012. A comparative study of the trabecular bony architecture of the talus in humans, non-human primates, and Australopithecus. Journal of Human Evolution 63, 536-551.

DeSilva, J.M., Gill, S.V., 2013. Brief communication: a midtarsal (midfoot) break in the human foot. American Journal of Physical Anthropology 151, 495-499.

DeSilva, J.M., Holt, K.G., Churchill, S.E., Carlson, K.J., Walker, C.S., Zipfel, B., et al., 2013. The lower limb and mechanics of walking in Australopithecus sediba. Science 340, 1232999.

DeSilva, J.M., Bonne-Annee, R., Swanson, Z., Gill, C.M., Sobel, M., Uy. J., Gill, S.V., 2015. Midtarsal break variation in modern humans: functional causes, skeletal correlates, and paleontological implications. American Journal of Physical Anthropology 156, 543-552.

DeSilva, J., McNutt, E., Benoit, J. and Zipfel, B., 2019. One small step: A review of Plio-Pleistocene hominin foot evolution. American Journal of Physical Anthropology 168, 63-140.

Devlin, M.J., 2011. Estrogen, exercise, and the skeleton. Evolutionary Anthropology 20, 54-61.

Devlin, M.J., Bouxsein, M.L., 2012. Influence of pre- and peri-natal nutrition on skeletal acquisition and maintenance. Bone 50, 444-451.

Devlin, M.J., Grasemann, C., Cloutier, A.M., Louis, L., Alm, C., Palmert, M.R., Bouxsein, M.L., 2013. Maternal perinatal diet induces developmental programming of bone architecture. Journal of Endocrinology 217, 69-81.

Doden, E., 1993. The relationship between the function and the inner cortical structure of metacarpal and phalangeal bones. In: Preuschoft, H., Chivers, D. J. (Eds.), Hands of Primates. Springer, Vienna, pp. 271-284.

Domínguez-Rodrigo, M., Pickering, T.R., Baquedano, E., Mabulla, A., Mark, D.F., Musiba, C., Bunn, H.T., Uribelarrea, D., Smith, V., Diez-Martin, F. Pérez-González, A., 2013. First partial skeleton of a 1.34-million-year-old Paranthropus boisei from Bed II, Olduvai Gorge, Tanzania. PLoS One 8, e80347.

Donahue, S.W., Sharkey, N.A. 1999. Strains in the metatarsals during the stance phase of gait: Implications for stress fractures. Journal of Bone Joint Surgery 81, 1236-1244.

Doran, D.M. 1993a. Comparative locomotor behavior of chimpanzees and bonobos - the influence of morphology on locomotion. American Journal of Physical Anthropology 91, 83-98.

Doran, D.M., 1997. Ontogeny of locomotion in mountain gorillas and chimpanzees. Journal of Human Evolution 32, 323-344.

Doube, M., Klosowski, M.M., Wiktorowicz-Conroy, A.M., Hutchinson, J.R., Shefelbine, S.J., 2011. Trabecular bone scales allometrically in mammals and birds. Proceedings of the Royal Society B - Biological Sciences 278, 3067-3073.

Dowdeswell, M.R., Jashashvili, T., Patel, B.A., Lebrun, R., Susman, R.L., Lordkipanidze, D., Carlson, K.J., 2017. Adaptation to bipedal gait and fifth metatarsal structural properties in Australopithecus, Paranthropus, and Homo. Comptes Rendus Palevol 16, 585-599.

Drapeau, M.S.M., Harmon, E.H., 2013. Metatarsal torsion in monkeys, apes, humans and Australopiths. Journal of Human Evolution 64, 93-108.

Dunmore, C.J., Wollny, G. Skinner, M.M., 2018. MIA-Clustering: a novel method for segmentation of paleontological material. PeerJ 6, e4374.

Efron, B., Tibshirani, R., 1993. An introduction to the bootstrap. CRC Press, LLC, Boca Raton, Florida.

Elftman, H., Manter, J., 1935. The evolution of the human foot, with especial reference to the joints. Journal of Anatomy 70, 56-67.

Eriksen, E.F., 2010. Cellular mechanisms of bone remodeling. Reviews in Endocrine and Metabolic Disorders 11, 219-227.

Fajardo, R.J., Muller, R., Ketcham, R.A., Colbert, M., 2007. Nonhuman anthropoid primate femoral neck trabecular architecture and its relationship to locomotor mode. Anatomical Record 290, 422-436.

Ferguson, W.W., 1989. A new species of the genus Australopithecus (primates: Hominidae) from Plio/Pleistocene deposits west of Lake Turkana in Kenya. Primates 30, 223-232.

Fernández, P.J., Almécija, S., Patel, B.A., Orr, C.M., Tocheri, M.W., Jungers, W.L., 2015. Functional aspects of metatarsal head shape in humans, apes, and old world monkeys. Journal of Human Evolution 86, 136-146.

Fox, J.C., Keaveny, T.M. 2001. Trabecular eccentricity and bone adaptation. Journal of Theoretical Biology 212, 211-221.

Gebo, D.L., 1996. Climbing, brachiation, and terrestrial quadrupedalism: Historical precursors of hominid bipedalism. American Journal of Physical Anthropology 101, 55-92.

Gebo, D.L., Schwartz, G.T. 2006. Foot bones from Omo: implications for hominid evolution. American Journal of Physical Anthropology 129, 499-511.

Gill, C.M., Bredella, M.A., DeSilva, J.M., 2015. Skeletal development of hallucal tarsometatarsal joint curvature and angulation in extant apes and modern humans. Journal of Human Evolution 88, 137-145.

Gosman, J.H., Ketcham, R.A., 2009. Patterns in ontogeny of human trabecular bone from SunWatch village in the prehistoric Ohio valley: General features of microarchitectural change. American Journal of Physical Anthropology 138, 318-332.

Green, D.J., Chirchir, H., Mbua, E., Harris, J.W., Braun, D.R., Griffin, N.L., Richmond, B.G., 2018. Scapular anatomy of Paranthropus boisei from Ileret, Kenya. Journal of Human Evolution 125, 181-192.

Griffin, N.L., D'Août, K., Richmond, B., Gordon, A., Aerts, P., 2010a. Comparative in vivo forefoot kinematics of Homo sapiens and Pan paniscus. Journal of Human Evolution 59, 608-619.

Griffin, N.L., D'Août, K., Ryan, T.M., Richmond, B.G., Ketcham, R.A., Postnov, A., 2010b. Comparative forefoot trabecular bone architecture in extant hominids. Journal of Human Evolution 59, 202-213.

Griffin, N.L., Richmond, B.G., 2005. Cross-sectional geometry of the human forefoot. Bone 37, 253-260.

Griffin, N.L., Richmond, B.G., 2010. Joint orientation and function in great ape and human proximal pedal phalanges. American Journal of Physical Anthropology 141, 116-123.

Griffin, N.L., Miller, C.E., Schmitt, D., D'Août, K., 2015. Understanding the evolution of the windlass mechanism of the human foot from comparative anatomy: Insights, obstacles, and future directions. American Journal of Physical Anthropology 156, 1-10.

Grine, F.E., Susman, R.L. 1991. Radius of Paranthropus robustus from Member 1, Swartkrans formation, South Africa. American Journal of Physical Anthropology 84, 229-248.

Grine, F.E. 1993. Description and preliminary analysis of new hominid craniodental fossils from the Swartkrans formation. Swartkrans: A Cave's Chronicle of Early Man.Transvaal Museum, Pretoria 75-116.

Grine, F.E., Daegling, D.J. 1993. New mandible of Paranthropus robustus from member 1, Swartkrans formation, South Africa. Journal of Human Evolution 24, 319-333.

Gross, T., Kivell T.L., Skinner, M.M., Nguyen, H., Pahr, D.H. 2014. A CT-image-based method for the holistic analysis of cortical and trabecular bone. Paleontologia Electronica 17, A17333.

Guldberg, R.E., Richards, M., Caldwell, N.J., Kuelske, C.L., Goldstein, S.A., 1997. Trabecular bone adaptation to variations in porous-coated implant topology. Journal of Biomechanics 30, 147-153.

Haile-Selassie, Y., Saylor, B.Z., Deino, A., Levin, N.E., Alene, M., Latimer, B.M., 2012. A new hominin foot from Ethiopia shows multiple Pliocene bipedal adaptations. Nature 483, 565-579.

Harcourt-Smith, W.E.H., O'Higgins, P., Aiello, L.C., 2002. From Lucy to Littlefoot: a three dimensional analysis of Plio-Pleistocene hominin tarsal remains. American Journal of Physical Anthropology S34, 82-82.

Harcourt-Smith, W.E.H., Aiello, L.C., 2004. Fossils, feet and the evolution of human bipedal locomotion. Journal of Anatomy 204, 403-416.

Harcourt-Smith, W.E.H., Throckmorton, Z., Congdon, K.A., Zipfel, B., Deane, A.S., Drapeau, M.S.M., Churchill, S.E., Berger, L.R., DeSilva, J.M., 2015. The foot of Homo naledi. Nature Communications 6, 8432.

Harrison, L.C., Nikander, R., Sikiö, M., Luukkaala, T., Helminen, M.T., Ryymin, P., Soimakallio, S., Eskola, H.J., Dastidar, P., Sievänen, H., 2011. MRI texture analysis of femoral neck: Detection of exercise load-associated differences in trabecular bone. Journal of Magnetic Resonance Imaging 34, 1359-1366.

Havill, L.M., Allen, M.R., Bredbenner, T.L., Burr, D.B., Nicolella, D.P., Turner, C.H., Warren, D.M., Mahaney, M.C., 2010. Heritability of lumbar trabecular bone mechanical properties in baboons. Bone 46, 835-840.

Hetherington, V.J., Carnett, J., Patterson, B.A. 1989. Motion of the first metatarsophalangeal joint. The Journal of Foot Surgery 28, 13-19.

Hicks, J.H., 1954. The mechanics of the foot: II. The plantar aponeurosis and the arch. Journal of Anatomy 88, 25-30.1.

Hodgskinson, R., Currey, J.D., 1990. Effects of structural variation on Young's modulus of non-human cancellous bone. Proceedings of the Institution of Mechanical Engineers Part H Journal of Engineering in Medicine 204, 43-52.

Huiskes, R., Ruimerman, R., van Lenthe, G., Janssen, J. 2000. Effects of mechanical forces on maintenance and adaptation of form in trabecular bone. Nature 405, 704-706.

Hunt, A.E., Smith, R.M., Torode, M., Keenan, A.M., 2001. Inter-segment foot motion and ground reaction forces over the stance phase of walking. Clinical Biomechanics 16, 592-600.

Hutton, W.C., Dhanendran, M., 1981. The mechanics of normal and hallux valgus feet – a quantitative study. Clinical Orthopaedics and Related Research 157, 7-13.

Inouye, S.E. 1992. Ontogeny and allometry of African ape manual rays. Journal of Human Evolution 23, 107-138.

Jacobs, C.R., 2000. The mechanobiology of cancellous bone structural adaptation. Journal of Rehabilitation Research and Development 37, 209-216.

Jashashvili, T., Dowdeswell, M.R., Lebrun, R., Carlson, K.J., 2015. Cortical structure of hallucal metatarsals and locomotor adaptations in hominoids. Plos One 10, e0117905.

Judex, S., Garman, R., Squire, M., Donahue, L.R., Rubin, C., 2004. Genetically based influences on the site-specific regulation of trabecular and cortical bone morphology. Journal of Bone and Mineral Research 19, 600-606.

Katoh, Y., Chao, E.Y., Laughman, R.K., Schneider, E., Morrey, B.F. (1983). Biomechanical analysis of foot function during gait and clinical applications. Clinical Orthopaedics and Related Research 177, 23-33.

Kidd, R.S., O'Higgins, P., Oxnard, C.E., 1996. The OH8 foot: a reappraisal of the functional morphology of the hindfoot utilizing a multivariate analysis. Journal of Human Evolution 31, 269-291.

Kivell, T.L., 2016. A review of trabecular bone functional adaptation: What have we learned from trabecular analyses in extant hominoids and what can we apply to fossils? Journal of Anatomy 228, 569-594.

Kraft, T.S., Venkataraman, V.V., Dominy, N.J. 2014. A natural history of human tree climbing. Journal of Human Evolution 71, 105-118.

Lambers, F.M., Koch, K., Kuhn, G., Ruffoni, D., Weigt, C., Schulte, F.A., Müller, R., 2013. Trabecular bone adapts to long-term cyclic loading by increasing stiffness and normalization of dynamic morphometric rates. Bone 55, 325-334.

Lanyon, L.E., 1973. Analysis of surface bone strain in the calcaneus of sheep during normal locomotion: strain analysis of the calcaneus. Journal of Biomechanics 6, 41-42.

Lanyon, L.E., 1974. Experimental support for the trajectorial theory of bone structure. Journal of Bone and Joint Surgery 56, 160-166.

Latimer, B.M., Lovejoy, C.O., Johanson, D.C., Coppens, Y. 1982. Hominid tarsal, metatarsal, and phalangeal bones recovered from the Hadar formation: 1974–1977 collections. American Journal of Physical Anthropology 57, 701-719.

Latimer, B.M., Lovejoy, C.O., 1990. Hallucal tarsometatarsal joint in Australopithecus afarensis. American Journal of Physical Anthropology 82, 125-133.

Lazenby, R.A., Skinner, M.M., Kivell, T.L., Hublin, J.-J., 2011. Scaling VOI size in 3D µCT studies of trabecular bone: A test of the over-sampling hypothesis. American Journal of Physical Anthropology 144, 196-203.

Leakey, L.S., Tobias, P.V., Napier, J.R., 1964. A new species of the genus Homo from Olduvai Gorge. Nature 202, 7-9.

Lee, C.R., Farley, C.T., 1998. Determinants of the center of mass trajectory in human walking and running. Journal of Experimental Biology 201, 2935-2944.

Legendre, P., 2018. lmodel2: Model II Regression. R package version 1.7-3.

Lieberman, D., 1996. How and why humans grow thin skulls: Experimental evidence for systemic cortical robusticity. American Journal of Physical Anthropology 101, 217-236.

Lisowski, F.P. 1967. Angular growth changes and comparisons in the primate talus. Folia Primatologica 7, 81-97.

Lorenzo, C., Arsuaga, J.L., Carretero, J.M. 1999. Hand and foot remains from the Gran Dolina Early Pleistocene site (Sierra de Atapuerca, Spain). Journal of Human Evolution 37, 501-522.

Lovejoy, C.O. 2009. Reexamining human origins in light of Ardipithecus ramidus. Science 326, 74-74e8.

MacLatchy, L., Muller, R., 2002. A comparison of the femoral head and neck trabecular architecture of Galago and Perodicticus using micro-computed tomography (µCT). Journal of Human Evolution 43, 89-105.

Maga, M., Kappelman, J., Ryan, T., Ketcham, R., 2006. Preliminary observations on the calcaneal trabecular microarchitecture of extant large-bodied hominoids. American Journal of Physical Anthropology 129, 410-417.

Maquer, G., Musy, S.N., Wandel, J., Gross, T., Zysset, P.K., 2015. Bone volume fraction and fabric anisotropy are better determinants of trabecular bone stiffness than other morphological variables. Journal of Bone Mineral Research 30, 1000-1008.

Marchi, D., 2005. The cross-sectional geometry of the hand and foot bones of the Hominoidea and its relationship to locomotor behavior. Journal of Human Evolution 49, 743-761.

Marchi, D., 2010. Articular to diaphyseal proportions of human and great ape metatarsals. American Journal of Physical Anthropology 143, 198-207.

McClure, N.K., Phillips, A.C., Vogel, E.R., Tocheri, M.W., 2012. Unexpected pollex and hallux use in wild Pongo pygmaeus wurmbii. American Journal of Physical Anthropology 54(S), 208.

McHenry, H.M., 1991. Petite bodies of the robust australopithecines. American Journal of Physical Anthropology 86, 445-454.

McHenry, H.M., Coffing, K. 2000. Australopithecus to Homo: transformations in body and mind. Annual Review of Anthropology 29, 125-146.

McHenry, H.M., Jones, A.L., 2006. Hallucial convergence in early hominids. Journal of Human Evolution 50, 534-539.

Midlo, C., 1934. Form of hand and foot in primates. American Journal of Physical Anthropology 19, 337-389.

Mittra, E., Rubin, C., Qin, Y., 2005. Interrelationship of trabecular mechanical and microstructural properties in sheep trabecular bone. Journal of Biomechanics 38, 1229-1237.

Morton, D.J., 1922. Evolution of the human foot. American Journal of Physical Anthropology 5, 305-336.

Morton, D.J., 1924. Evolution of the human foot II. American Journal of Physical Anthropology 7, 1-52.

Mullender, M.G., Huiskes, R., Versleyen, H., Buma, P. 1996. Osteocyte density and histomorphometric parameters in cancellous bone of the proximal femur in five mammalian species. Journal of Orthopaedic Research 14, 972-979.

Munro, C.F., Miller, D.I., Fuglevand, A.J., 1987. Ground reaction forces in running: a reexamination. Journal of Biomechanics 20, 147-155.

Napier, J.R., 1964. The evolution of bipedal walking in the hominids. Archives of Biological Sciences 37, 3.

Nester, C., Jones, R.K., Liu, A., Howard, D., Lundberg, A., Arndt, A., Stacoff, A. Wolf, P., 2007. Foot kinematics during walking measured using bone and surface mounted markers. Journal of Biomechanics 40, 3412.

Odgaard, A., 1997. Three-dimensional methods for quantification of cancellous bone architecture. Bone 20, 315-328.

Oishi, M., Ogihara, N., Endo, H., Une, Y., Ichihara, N., Asari, M., Amasaki, H., 2012. Muscle dimensions of the foot in the orangutan and the chimpanzee. Journal of Anatomy 221, 311-317.

Pahr, D.H., Zysset, P.K., 2009. From high-resolution CT data to finite element models: Development of an integrated modular framework. Computer Methods in Biomechanics and Biomedical Engineering 12, 45-57.

Pickering, R., Kramers, J.D., 2010. Re-appraisal of the stratigraphy and determination of new U-Pb dates for the Sterkfontein hominin site, South Africa. Journal of Human Evolution 59, 70-86.

Polk, J.D., Blumenfeld, J., Ahluwalia, D., 2008. Knee posture predicted from subchondral apparent density in the distal femur: an experimental validation. The Anatomical Record: Advances in Integrative Anatomy and Evolutionary Biology 291, 293-302.

Pontzer, H., Lieberman, D., Momin, E., Devlin, M., Polk, J., Hallgrimsson, B., Cooper, D.M.L., 2006. Trabecular bone in the bird knee responds with high sensitivity to changes in load orientation. Journal of Experimental Biology 209, 57-65.

Pontzer, H., Rolian, C., Rightmire, G.P., Jashashvili, T., Ponce de León, M.S., Lordkipanidze, D., Zollikofer, C.P., 2010. Locomotor anatomy and biomechanics of the Dmanisi hominins. Journal of Human Evolution 58, 492-504.

Proctor, D.J., 2010. Brief communication: Shape analysis of the MT 1 proximal articular surface in fossil hominins and shod and unshod Homo. American Journal of Physical Anthropology 143, 631-637.

Proctor, D.J., Broadfield, D., Proctor, K., 2008. Quantitative three-dimensional shape analysis of the proximal hallucial metatarsal articular surface in Homo, Pan, Gorilla, and Hylobates. American Journal of Physical Anthropology 135, 216-224.

Raichlen, D.A., Gordon, A.D., Foster, A.D., Webber, J.T., Sukhdeo, S.M., Scott, R.S., Gosman, J.H., Ryan, T.M., 2015. An ontogenetic framework linking locomotion and trabecular bone architecture with applications for reconstructing hominin life history. Journal of Human Evolution 81, 1-12.

Rafferty, K.L. and Ruff, C.B., 1994. Articular structure and function in *Hylobates*, *Colobus*, and *Papio*. American Journal of Physical Anthropology 94, 395-408.

Räth, C., Baum, T., Monetti, R., Sidorenko, I., Wolf, P., Eckstein, F., Matsuura, M., Lochmüller, E.M., Zysset, P.K., Rummeny, E.J. and Link, T.M., 2013. Scaling relations between trabecular bone volume fraction and microstructure at different skeletal sites. Bone 57, 377-383.

Remis, M.J., 1995. Effects of body size and social context on the arboreal activities of lowland gorillas in the Central African Republic. American Journal of Physical Anthropology 97, 413-433.

Remis, M.J., 1999. Tree structure and sex differences in arboreality among western lowland gorillas (Gorilla gorilla gorilla) at Bai Hokou, Central African Republic. Primates 40, 383-396.

Richmond, B.G. 2007. Biomechanics of phalangeal curvature. Journal of Human Evolution 53, 678-690.

Robinson, J.T. 1972. Early hominid posture and locomotion. University of Chicago Press.

Rodgers, M.M. 1995. Dynamic foot biomechanics. Journal of Orthopaedic and Sports Physical Therapy 21, 306-316.

RStudio Team (2015). RStudio: Integrated Development for R. RStudio, Inc., Boston.

Rubin, C., Turner, A.S., Mallinckrodt, C., Jerome, C., Mcleod, K., Bain, S., 2002. Mechanical strain, induced noninvasively in the high-frequency domain, is anabolic to cancellous bone, but not cortical bone. Bone 30, 445-452.

Ruff, C., 1983. The contribution of cancellous bone to long-bone strength and rigidity. American Journal of Physical Anthropology 61, 141-143.

Ruff, C., Runestad, J., 1992. Primate limb bone structural adaptations. Annual Review of Anthropology 21, 407-433.

Ruff, C., Holt, B., Trinkaus, E., 2006. Who's afraid of the big bad Wolff? Wolff’s Law and bone functional adaptation. American Journal of Physical Anthropology 129, 484-498.

Ryan, T.M., Ketcham, R.A., 2002. The three-dimensional structure of trabecular bone in the femoral head of strepsirrhine primates. Journal of Human Evolution 43, 1-26.

Ryan, T.M., Ketcham, R.A., 2005. Angular orientation of trabecular bone in the femoral head and its relationship to hip joint loads in leaping primates. Journal of Morphology 265, 249-263.

Ryan, T.M., Krovitz, G.E., 2006. Trabecular bone ontogeny in the human proximal femur. Journal of Human Evolution 51, 591-602.

Ryan, T.M., Walker, A., 2010. Trabecular bone structure in the humeral and femoral heads of anthropoid primates. Anatomical Record 293, 719-729.

Ryan, T.M., Shaw, C.N., 2012. Unique suites of trabecular bone features characterize locomotor behavior in human and non-human anthropoid primates. Plos One 7, e41037.

Ryan, T.M., Shaw, C.N., 2013. Trabecular bone microstructure scales allometrically in the primate humerus and femur. Proceedings of the Royal Society B: Biological Sciences 280, 20130172.

Ryan, T.M., Shaw, C.N., 2015. Gracility of the modern Homo sapiens skeleton is the result of decreased biomechanical loading. Proceedings of the National Academy of Sciences 112, 372-377.

Saers, J.P.P, Cazorla-Bak, Y., Shaw, C.N., Stock, J.T., Ryan, T.M., 2016. Trabecular bone structural variation throughout the human lower limb. Journal of Human Evolution 97, 97-108.

Saers, J.P.P., 2017. Ontogeny and functional adaptation of trabecular bone in the human foot. Ph.D. Dissertation, University of Cambridge.

Saparin, P., Scherf, H., Hublin, J.-J., Fratzl, P., Weinkamer, R. 2011. Structural adaptation of trabecular bone revealed by position resolved analysis of proximal femora of different primates. The Anatomical Record 294, 55-67.

Sarmiento, E. 1994. Terrestrial traits in the hands and feet of gorillas. American Museum Novitates 3091, New York: American Museum of Natural History.

Sarringhaus, L.A., MacLatchy, L.M., Mitani, J.C., 2014. Locomotor and postural development of wild chimpanzees. Journal of Human Evolution 66, 29-38.

Scherf, H., Harvati, K., Hublin, J.-J., 2013. A comparison of proximal humeral cancellous bone of great apes and humans. Journal of Human Evolution 65, 29-38.

Scherf, H., Tilgner, R., 2009. A new high-resolution computed tomography (CT) segmentation method for trabecular bone architectural analysis. American Journal of Physical Anthropology 140, 39-51.

Shaw, C.N., Stock, J.T., 2009a. Habitual throwing and swimming correspond with upper limb diaphyseal strength and shape in modern human athletes. American Journal of Physical Anthropology 140, 160-172.

Shaw, C.N., Stock, J.T., 2009b. Intensity, repetitiveness, and directionality of habitual adolescent mobility patterns influence the tibial diaphysis morphology of athletes. American Journal of Physical Anthropology 140, 149-159.

Shaw, C.N., Ryan, T.M., 2012. Does skeletal anatomy reflect adaptation to locomotor patterns? Cortical and trabecular architecture in human and nonhuman anthropoids. American Journal of Physical Anthropology 147, 187-200.

Shaw, C.N., Stock, J.T., 2013. Extreme mobility in the Late Pleistocene? Comparing limb biomechanics among fossil *Homo*, varsity athletes and Holocene foragers. Journal of Human Evolution 64, 242-249.

Shea, B.T. 1981. Relative growth of the limbs and trunk in the African apes. American Journal of Physical Anthropology 56, 179-201.

Simkin, A., Ayalon, J., Leichter, I., 1987. Increased trabecular bone density due to bone-loading exercises in postmenopausal osteoporotic women. Calcified Tissue International 40, 59-63.

Sinclar, K.D., Farnsworth, R.W., Pham, T.X., Knight, A.N., Bloebaum, R.D., Skedros, J.G., 2013. The artiodactyl calcaneus as a potential 'control bone' cautions against simple interpretations of trabecular bone adaptation in the anthropoid femoral neck. Journal of Human Evolution 64, 366-379.

Skedros, J.G., Hunt, K.J., Bloebaum, R.D., Relationships of loading history and structural and material characteristics of bone: development of the mule deer calcaneus. Journal of Morphology 259, 281-307.

Skerry, T., Lanyon, L., 1995. Interruption of disuse by short-duration walking exercise does not prevent bone loss in the sheep calcaneus. Bone 16, 269-274.

Soames, R.W., 1985. Foot pressure patterns during gait. Journal of Biomedical Engineering 7, 120-126.

Stern, J.T., Susman, R.L., 1983. The locomotor anatomy of Australopithecus afarensis. American Journal of Physical Anthropology 60, 279-317.

Stern, J.T. 2000. Climbing to the top: A personal memoir of *Australopithecus afarensis*. Evolutionary Anthropology 9, 113-133.

Stokes, I.A., Hutton, W.C., Stott, J.R., 1979. Forces acting on the metatarsals during normal walking. Journal of Anatomy 129, 579-590.

Su, A., Carlson, K.J., 2017. Comparative analysis of trabecular bone structure and orientation in South African hominin tali. Journal of Human Evolution 106, 1-18.

Sugiyama, T., Price, J.S., Lanyon, L.E., 2010. Functional adaptation to mechanical loading in both cortical and cancellous bone is controlled locally and is confined to the loaded bones. Bone 46, 314-321.

Susman, R.L., 1983. Evolution of the human foot - evidence from Plio-Pleistocene hominids. Foot and Ankle 3, 365-376.

Susman, R L., Stern, J.T., Jungers, W.L. 1984. Arboreality and bipedality in the Hadar hominids. Folia Primatologica 43, 113-156.

Susman, R.L., Brain, T.M., 1988. New first metatarsal (SKX 5017) from Swartkrans and the gait of Paranthropus robustus. American Journal of Physical Anthropology 77, 7-15.

Susman, R.L., de Ruiter, D.J., 2004. New hominin first metatarsal (SK 1813) from Swartkrans. Journal of Human Evolution 47, 171-181.

Sutherland, D.H., Olshen, R., Cooper, L., Woo, S.L., 1980. The development of mature gait. Gait and Posture 6, 163-170.

Swartz, S., Parker, A., Huo, C. 1998. Theoretical and empirical scaling patterns and topological homology in bone trabeculae. Journal of Experimental Biology 201, 573-590.

Thorpe, S.K.S., Crompton, R.H., 2005. Locomotor ecology of wild orangutans (Pongo pygmaeus abelii) in the Gunung Leuser ecosystem, Sumatra, Indonesia: A multivariate analysis using log-linear modelling. American Journal of Physical Anthropology 127, 58-78.

Tocheri, M.W., Solhan, C.R., Orr, C.M., Femiani, J., Frohlich, B., Groves, C. P., Harcourt-Smith, W.E., Richmond, B.G., Shoelson, B., Jungers, W.L., 2011. Ecological divergence and medial cuneiform morphology in gorillas. Journal of Human Evolution 60, 171-184.

Trinkaus, E. 1983. Functional-aspects of Neandertal pedal remains. Foot and Ankle 6, 377-390.

Tsegai, Z.J., Kivell, T.L., Gross, T., Nguyen, N.H., Pahr, D.H., Smaers, J.B., Skinner, M.M., 2013. Trabecular bone structure correlates with hand posture and use in hominoids. Plos One 8, e78781.

Tsegai, Z.J., Skinner, M.M., Gee, A.H., Pahr, D.H., Treece, G.M., Hublin, J.-J., Kivell, T.L., 2017. Trabecular and cortical bone structure of the talus and distal tibia in Pan and Homo. American Journal of Physical Anthropology 163, 784-805.

Tuttle, R.H., 1969. Quantitative and functional studies on the hands of the Anthropoidea. I. The Hominoidea. Journal of Morphology 128, 309-363.

Tuttle, R.H. 1981. Evolution of hominid bipedalism and prehensile capabilities. Philosophical Transactions of the Royal Society B 292, 89-94.

Tuttle, R.H., Rogers, C.M., 1966. Genetic and selective factors in reduction of the hallux in Pongo pygmaeus. American Journal of Physical Anthropology 24, 191-198.

Vereecke, E., D'Août, K., Clercq, D.D., Elsacker, L.V., Aerts, P., 2003. Dynamic plantar pressure distribution during terrestrial locomotion of bonobos (Pan paniscus). American Journal of Physical Anthropology 120, 373-383.

Vernon, D.S., 2013. A morphometric analysis of the phalanges and a fragmentary first metatarsal from the Drimolen hominin site, South Africa. MPhil Dissertation, University of Johannesburg.

Wallace, I.J., Kwaczala, A.T., Judex, S., Demes, B., Carlson, K.J., 2013. Physical activity engendering loads from diverse directions augments the growing skeleton. Journal of Musculoskeletal and Neuronal Interactions 13, 283-288.

Ward, C.V., 2002. Interpreting the posture and locomotion of Australopithecus afarensis: Where do we stand? American Journal of Physical Anthropology 119, 185-215.

Ward, C.V., Kimbel, W.H. and Johanson, D.C., 2011. Complete fourth metatarsal and arches in the foot of *Australopithecus afarensis*. Science 331, 750-753.

White, T.D., Suwa, G., Asfaw, B. 1994. *Australopithecus ramidus*, a new species of early hominid from Aramis, Ethiopia. Nature 371, 306-312.

White, T.D., Lovejoy, C.O., Asfaw, B., Carlson, J.P., Suwa, G. 2015. Neither chimpanzee nor human, *Ardipithecus* reveals the surprising ancestry of both. Proceedings of the National Academy of Sciences 112, 4877-4884.

Whitehouse, W.J., 1974. The quantitative morphology of anisotropic trabecular bone. Journal of Microscopy-Oxford 101, 153-168.

Wickham, H. 2009. ggplot2: Elegant Graphics for Data Analysis. New York: Springer-Verlag.

Wood, B., Constantino, P. 2007. *Paranthropus boisei*: Fifty years of evidence and analysis. American Journal of Physical Anthropology 134, 106-132.

Wunderlich, R.E., Ischinger, S.B., 2017. Foot use during vertical climbing in chimpanzees (Pan troglodytes). Journal of Human Evolution 109, 1-10.

Zeininger, A., Patel, B.A., Zipfel, B., Carlson, K.J., 2016. Trabecular architecture in the StW 352 fossil hominin calcaneus. Journal of Human Evolution 97, 145-158.

Zeininger, A., Schmitt, D., Jensen, J.L., Shapiro, L.J., Ontogenetic changes in foot strike pattern and calcaneal loading during walking in young children. Gait and Posture 59, 18-22.

Zipfel, B., Kidd, R.S., 2006. Hominin first metatarsals (SKX 5017 and SK 1813) from Swartkrans: A morphometric analysis. Homo 57, 117-131.

Zipfel, B., DeSilva, J. M., Kidd, R.S. 2009. Earliest complete hominin fifth metatarsal—implications for the evolution of the lateral column of the foot. American Journal of Physical Anthropology 140, 532-545.

Zipfel, B., DeSilva, J.M., Kidd, R.S., Carlson, K.J., Churchill, S.E., Berger, L.R., 2011. The foot and ankle of Australopithecus sediba. Science 333, 1417-1420.

Figures and tables

Table 1. Study sample composition

Taxon	Side (R/L)	Sex (M/F/?)	Locomotor mode
Pongo pygmaeus	6 (3/3)	1/4/1	Suspensory (torso-orthogrady)
Gorilla gorilla	10 (6/4)	5/5/0	Arboreal/ terrestrial knuckle-walker
Pan troglodytes	10 (5/5)	6/4/0	Arboreal/ terrestrial knuckle-walker
Homo sapiens	11 (9/2)	6/5/0	Bipedal
Paranthropus robustus (?) SKX 5017	(0/1)		Bipedal/arboreal (?)
SK 1813 (Hominin indet.)	(1/0)		Bipedal/arboreal (?)

Table 2. Results from reduced major axis regression analysis. Displayed are all trabecular paramaters analyzed and their relationship to size. Included are bone volume fraction (BV/TV), trabecular thickness (Tb. Th.), trabecular spacing (Tb. Sp.), trabecular number (Tb. N.), and degree of anisotropy (DA). CL- and CL+ represent confidence limits for 95% intervals, and results indicate positive versus negative size-related correlation. (*) Asterisks denote that the isometric slope is contained within the CLs, and isometric scaling cannot be rejected.

	variable	Isometric slope value	slope	CL -	CL +	y-int	R^2	p-value	result
Pongo									
	BV/TV	0	1.94	0.66	5.69	-6.61	0.13	0.48	+
	Tb.Th	1	1.27	0.44	3.62	-4.97	0.18	0.39	+
	Tb.Sp	1	-1.28	-3.81	-0.43	3.14	0.09	0.56	-
	Tb.N	0	0.54	0.18	1.68	-1.39	0.01	0.88	+
	DA	0	1.40	0.45	4.31	-5.28	0.01	0.84	+
Gorilla									
	BV/TV	0	0.89	0.43	1.81	-3.96	0.09	0.40	+
	Tb.Th	1	1.18	0.70	1.98	-5.05	0.56	**0.01**	+*
	Tb.Sp	1	1.43	0.69	2.98	-4.89	0.03	0.62	+*
	Tb.N	0	-0.99	-1.91	-0.51	3.17	0.24	0.16	-
	DA	0	1.15	0.63	2.11	-4.89	0.37	0.06	+
Pan									
	BV/TV	0	-1.42	-2.90	-0.69	3.35	0.08	0.42	-
	Tb.Th	1	1.87	0.92	3.79	-7.13	0.12	0.33	+*
	Tb.Sp	1	3.21	1.90	5.41	-10.39	0.55	**0.01**	+
	Tb.N	0	-2.10	-3.74	-1.18	6.66	0.44	**0.04**	-
	DA	0	1.25	0.59	2.63	-4.90	<0.01	0.94	+
Homo									
	BV/TV	0	2.74	1.37	5.49	-10.42	<0.01	0.82	+
	Tb.Th	1	1.41	0.72	2.75	-6.17	0.08	0.39	+*
	Tb.Sp	1	2.56	1.28	5.13	-8.92	<0.01	0.85	+
	Tb.N	0	-1.84	-3.67	-0.92	6.23	0.01	0.78	-
	DA	0	1.26	0.65	2.41	-5.07	0.14	0.26	+

Table 3. Summary statistics for all analyzed parameters and taxa.

		Pongo pygmaeus	Gorilla gorilla	Pan troglodytes	SKX 5017	SK 1813	Homo sapiens
	BV/TV						
Head	Mean	0.32 ± 0.07	0.35 ± 0.05	0.38 ± 0.02	0.41	0.36	0.29 ± 0.04
	Range	0.19 - 0.23	0.28 - 0.421	0.29 - 0.44			0.23 - 0.34
	CV	22.70	13.10	13.40			15.50
Base	Mean	0.32 ± 0.09	0.33 ± 0.02	0.35 ± 0.03	0.38		0.24 ± 0.05
	Range	0.252- 0.47	0.28 - 0.37	0.31 - 0.40			0.16 - 0.33
	CV	26.80	7.00	7.80			30.00
	DA						
Head	Mean	0.24 ± 0.03	0.30 ± 0.04	0.33 ± 0.04	0.27	0.20	0.40 ± 0.04
	Range	0.19 - 0.28	0.25 - 0.35	0.27 - 0.39			0.33 - 0.46
	CV	13.10	12.80	12.60			9.00
Base	Mean	0.28	0.33 ± 0.04	0.37 ± 0.02	0.37		0.40 ± 0.04
	Range	0.19 - 0.34	0.25 - 0.40	0.35 - 0.41			0.34 - 0.45
	CV	18.50	13.00	5.30			8.90
	Trabecular thickness (mm)						
Head	Mean	0.26 ± 0.04	0.31 ± 0.04	0.29 ± 0.04	0.30	0.26	0.24 ± 0.02
	Range	0.20 - 0.31	0.26 - 0.37	0.22 - 0.34			0.20 - 0.29
	CV	16.90	12.00	14.00			10.50
Base	Mean	0.24 ± 0.04	0.28 ± 0.04	0.23 ± 0.02	0.25		0.20 ± 0.02
	Range	0.21 - 0.31	0.22 - 0.34	0.19 - 0.26			0.17 - 0.24
	CV	14.60	14.00	10.10			9.80
	Trabecular number (mm^{-1})						
Head	Mean	1.08 ± 0.07	0.88 ± 0.12	1.05 ± 0.20	1.15	1.32	1.13 ± 0.13
	Range	1.02 - 1.21	0.72 - 1.03	0.80 - 1.44			0.97 - 1.39
	CV	6.30	14.00	19.70			11.40
Base	Mean	1.21 ± 0.09	1.11 ± 0.11	1.39 ± 0.12	1.32		1.24 ± 0.17
	Range	1.11 - 1.34	0.99 - 1.34	1.23 - 1.58			0.91 - 1.51
	CV	7.60	9.70	8.90			13.60
	Trabecular spacing (mm)						
Head	Mean	0.70 ± 0.11	0.91 ± 0.20	0.75 ± 0.21	0.57	0.50	0.66 ± 0.10
	Range	0.53	0.69 - 1.19	0.48 - 1.12			0.49 - 0.82
	CV	15.80	22.00	28.10			14.90
Base	Mean	0.58 ± 0.09	0.63 ± 0.05	0.49 ± 0.05	0.50		0.63 ± 0.14
	Range	0.45 - 0.66	0.53 - 0.71	0.43 - 0.57			0.48 - 0.93
	CV	15.00	8.20	9.40			21.80

Table 4. Results from Kruskal-Wallis post hoc tests in interspecies BV/TV and DA ratio. Values above grey boxes represent the head and values below grey boxes represent the base.

	Pongo	Gorilla	Pan	Homo
BV/TV				
Pongo		0.029	0.560	<0.001
Gorilla	1.000		1.000	<0.001
Pan	1.000	1.000		<0.001
Homo	<0.001	<0.001	<0.001	
DA				
Pongo		1.000	1.000	1.000
Gorilla	0.045		1.000	1.000
Pan	0.252	1.000		0.690
Homo	1.000	0.214	1.000	

Table 5. Kruskal-Wallis post hoc test of interspecies absolute DA values. Values above grey diagonal boxes represent head, values below represent the base.

	Pongo	Gorilla	Pan	Homo
Pongo		0.096	<0.01	<0.001
Gorilla	0.707		0.993	<0.001
Pan	<0.01	<0.05		<0.01
Homo	<0.01	<0.01	0.910	

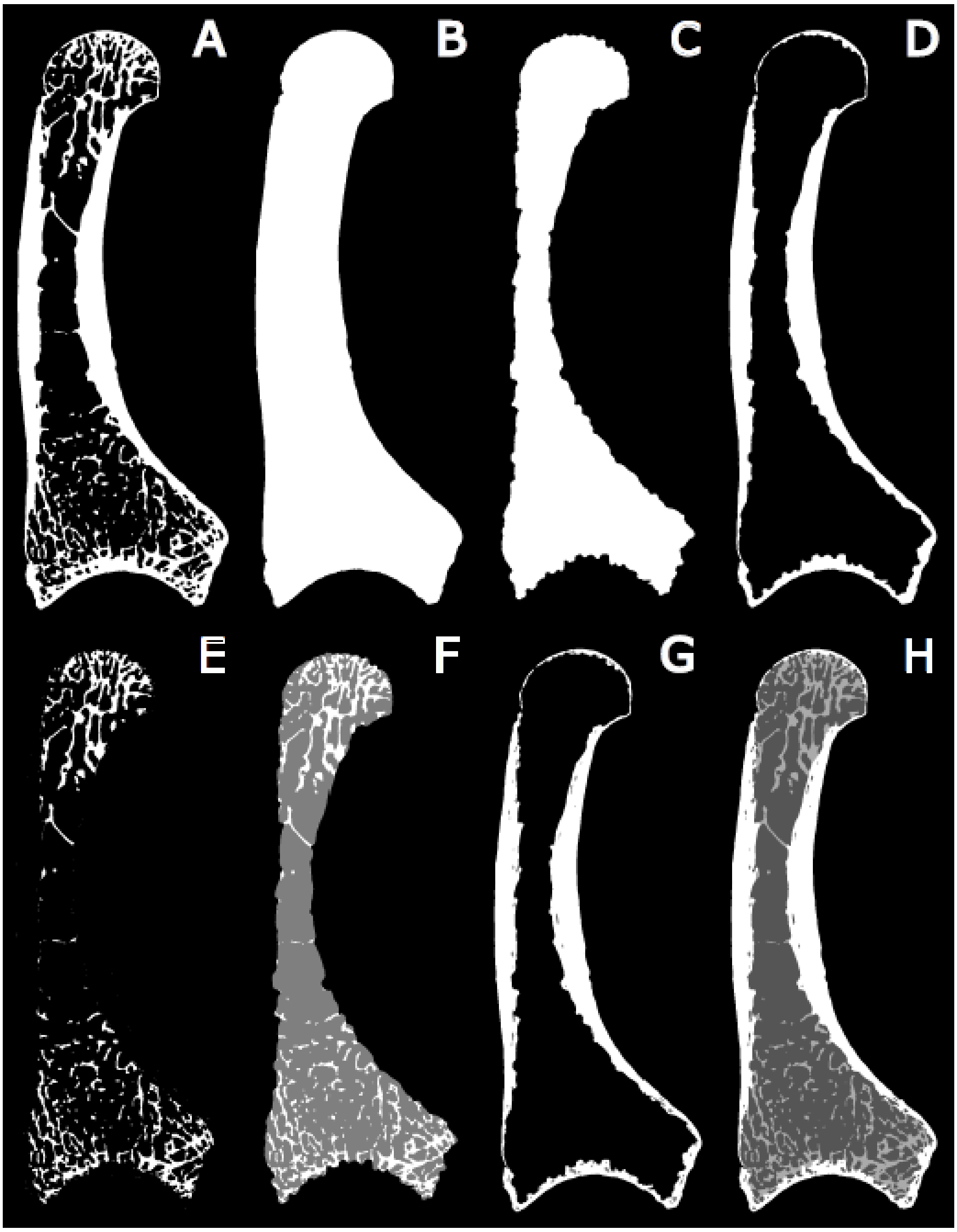

Figure 1. Masking procedure used to segment different components of bone. Illustrated here is a Gorilla first metatarsal that has undergone complete segmentation. From left to right: (a) segmented image; (b) outer mask; (c) inner mask; (d) cortical mask; (e) trabeculae only image; (f) MaskSeg In; (g) MaskSeg Out; (h) MaskSeg (this is the mask which is used for trabecular quantification by medtool).

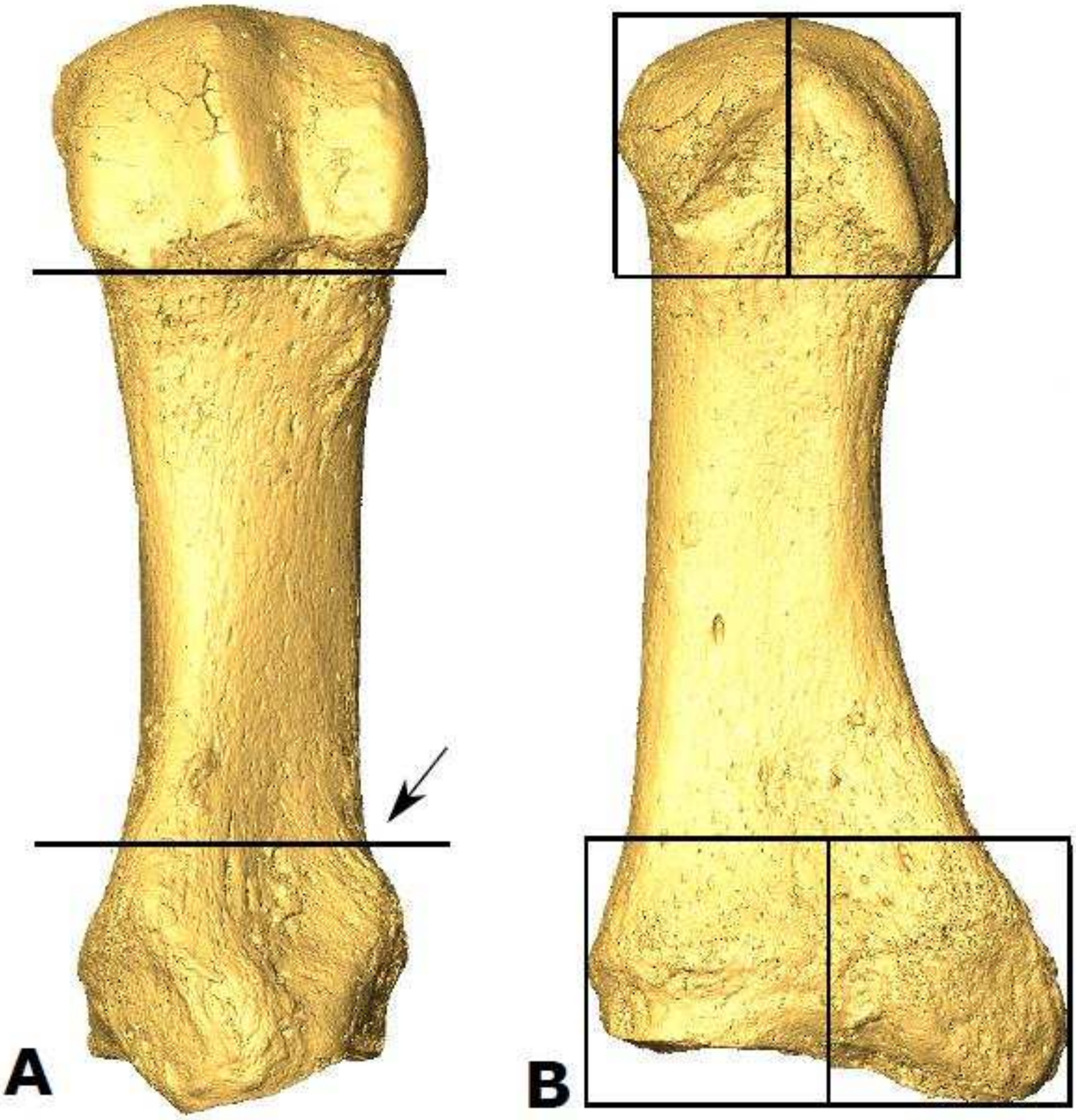

Figure 2. Delineation of the epiphyses and the dorsal and plantar sections. (a) The head was delineated where the articular surface terminates on the plantar aspect of the bone. Proximally, the base was delineated based on a homologous curvature on the medial aspect of the shaft (indicated by the arrow). (b) Both the base and the head were separated into dorsal and plantar sections by dividing in half the maximum dorso-plantar width.

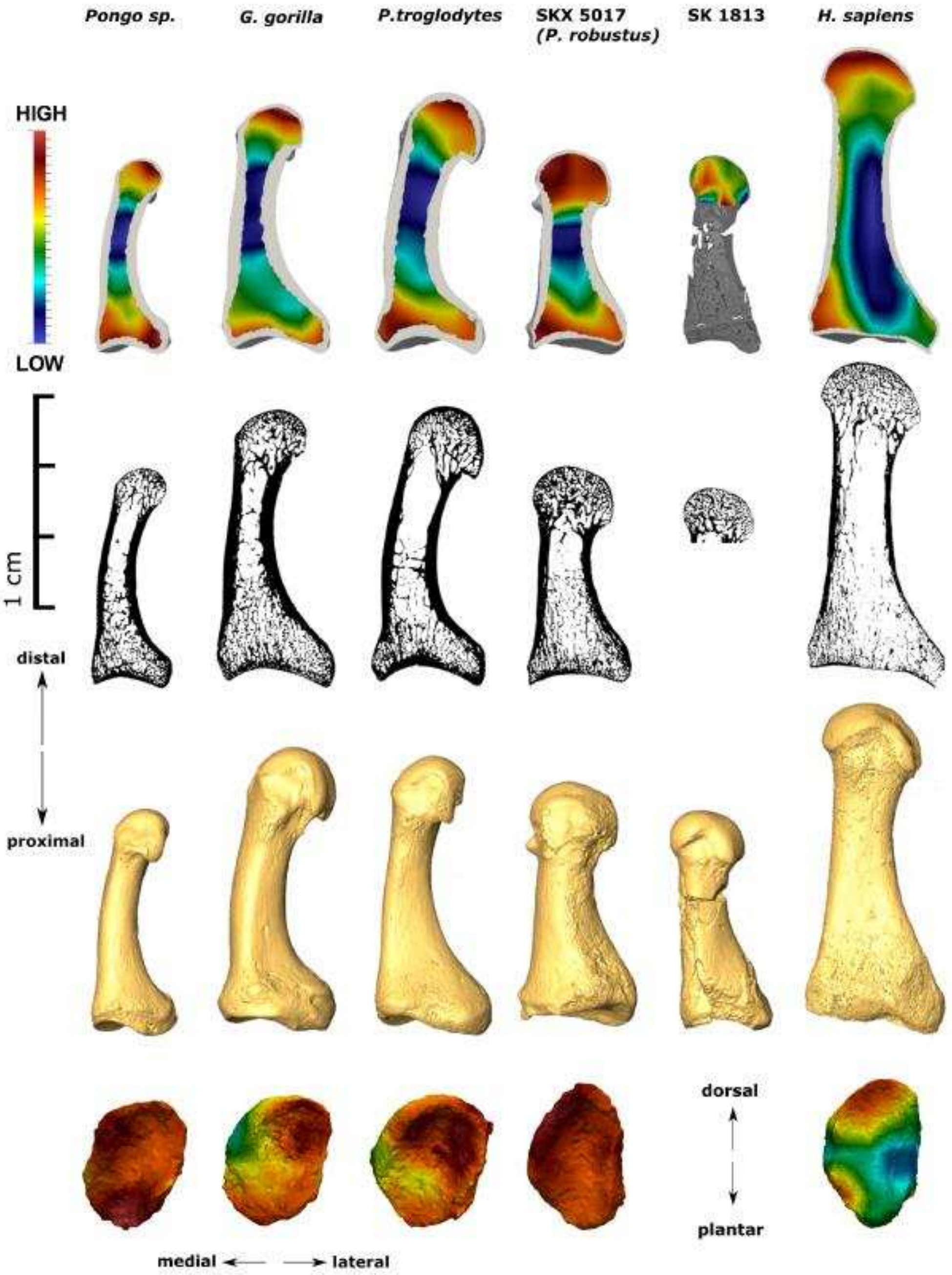

Figure 3. Representative specimens from each taxon. From top to bottom: BV/TV color maps of MT1 sagittal cross-section, segmented images, isosurfaces of external bone, and BV/TV color maps of proximal articular surfaces. BV/TV color maps are scaled to individual specimen ranges to visualize patterns of trabecular distribution as opposed to overall differences in BV/TV values. The first three rows are scaled to represent actual size differences between taxa. The color maps on the fourth row are all scaled to the same size, and do not represent natural size. SKX 5017 base on bottom row is mirrored to match the side of all other specimens.

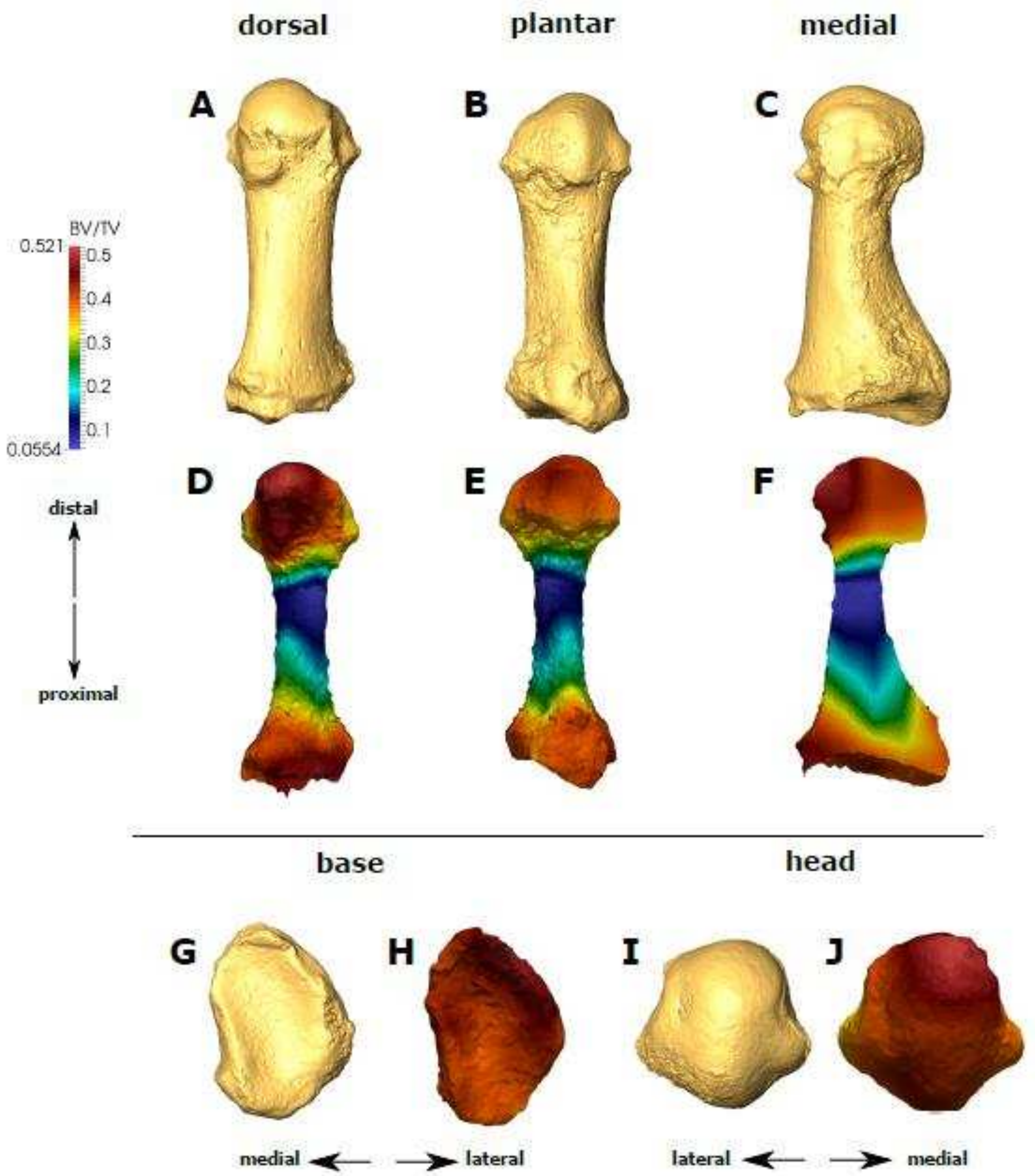

Figure 4. SKX 5017. Isosurfaces showing the external morphology of the element (a, b, c, g, i), and color maps of trabecular bone BV/TV (d, e, f, h, j). Images over the line show overall trabecular distribution throughout the whole bone in different positions, and images below the line display the dorso-plantar trabecular distribution in the epiphyses.

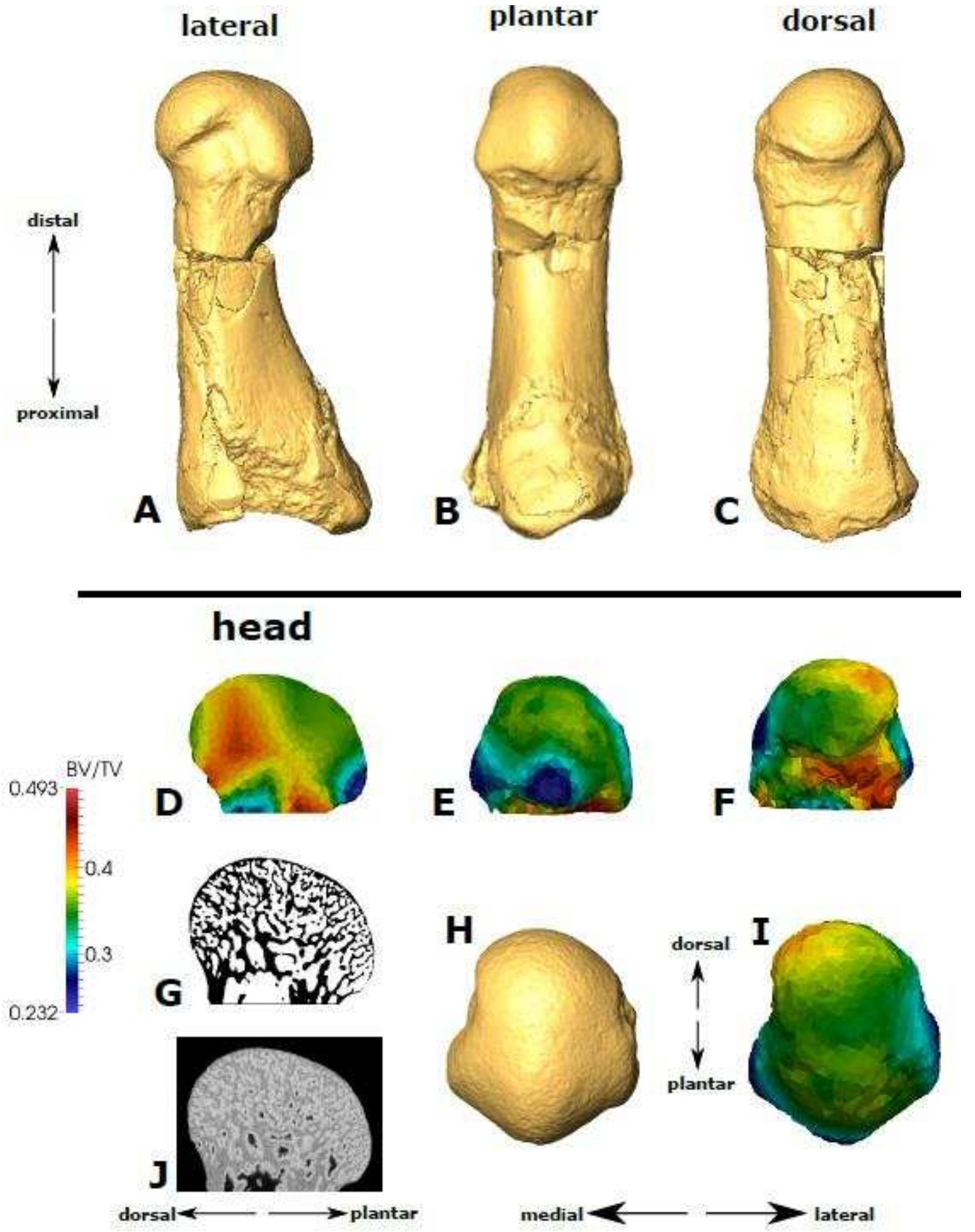

Figure 5. SK 1813. Isosurfaces showing the external morphology of the element (a, b, c, h). Images a, b, and c display the damage to the shaft and proximal aspect of the bone. Below the line are various visualizations of the metatarsal head. Illustrated are color maps of trabecular bone BV/TV (d, e, f, i). Notice the relatively dorsal position of high BV/TV, which is most clearly seen in the sagittal cross-section (d). This is also noticeable when viewing the element on its plantar (e), dorsal (f), and distal aspects (i). Also shown is the segmentation (g), and the original CT scan (j) of the head.

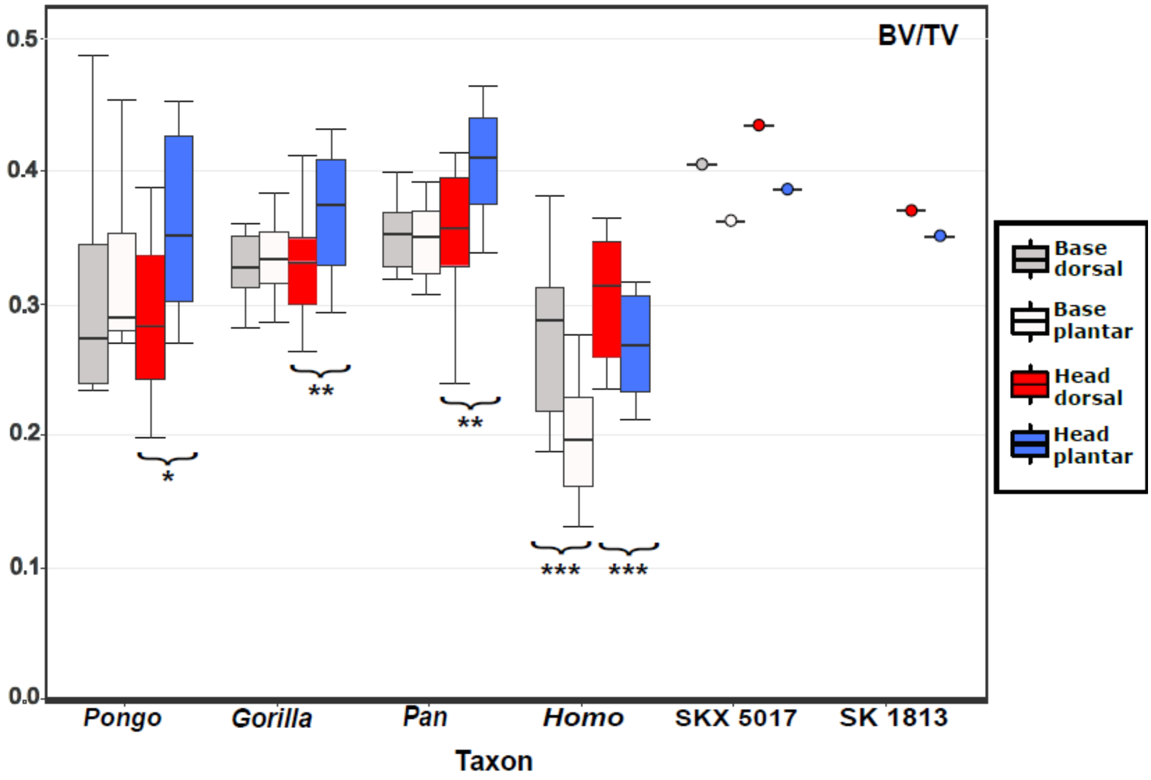

Figure 6. Boxplot showing raw BV/TV values within each analyzed region and each taxon. Significant differences in pairwise comparisons are denoted using asterisks [(*) = p<0.05; (**) = p<0.005; (***) = p<0.001)]. Within the base none of the non-human apes show significant differences between dorsal and plantar regions, whereas modern humans do. All taxa show significant differences between the dorsal and plantar regions of the head.

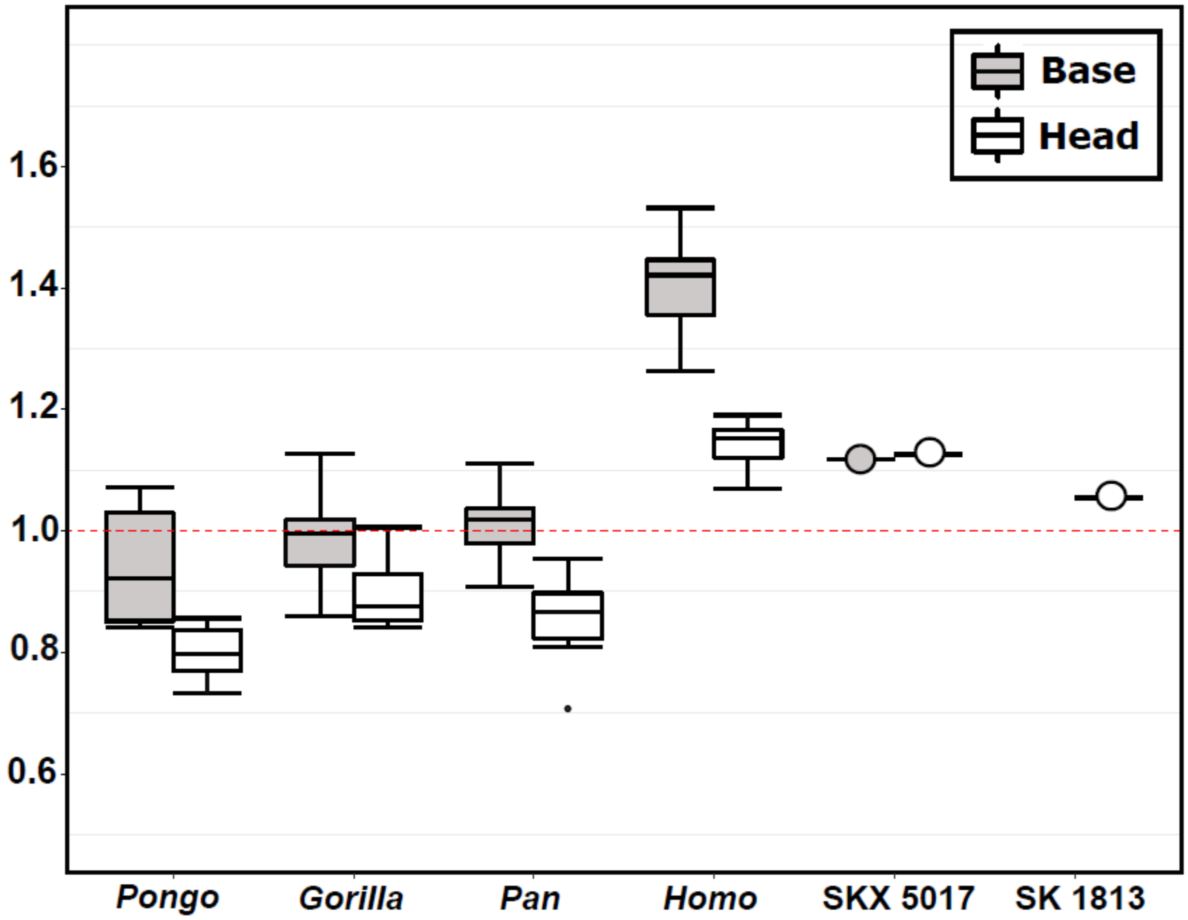

Figure 7. Boxplot of BV/TV ratio within the base and head of each taxon. Ratio represents the relative trabecular distribution; this is obtained by dividing dorsal values by plantar values and multiplying by 100. A ratio over one represents a more dorsal distribution and a ratio under one represents a more plantar distribution. Red dotted line represents an equal dorso-plantar distribution of trabecular bone.

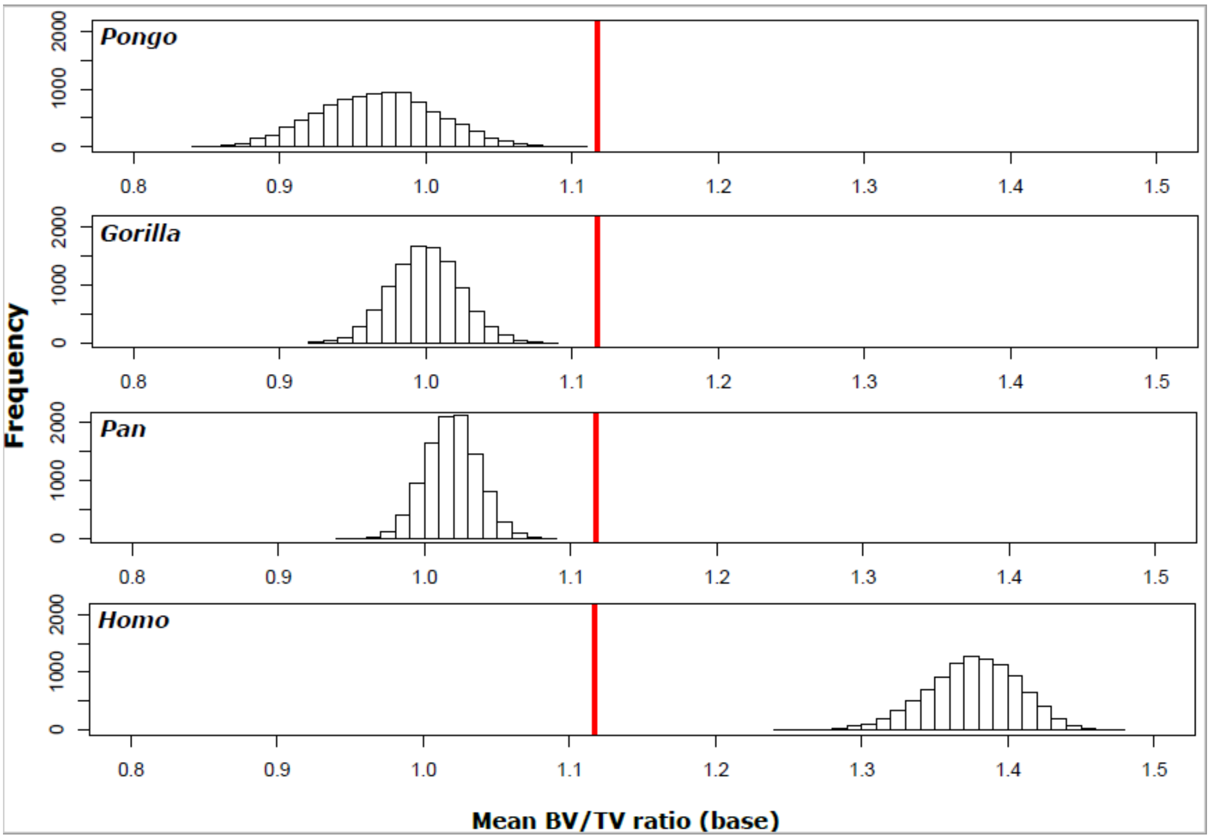

Figure 8. Bootstrap plots showing the resampled and redistributed sample means of BV/TV ratio within the base of each taxon. The red line represents the original BV/TV ratio of SKX 5017. Its position in the histograms represents the likelihood that the mean BV/TV ratio of the fossil hominins will fall within the range seen in modern taxa. In all cases, the red line falls outside the range of modern taxa.

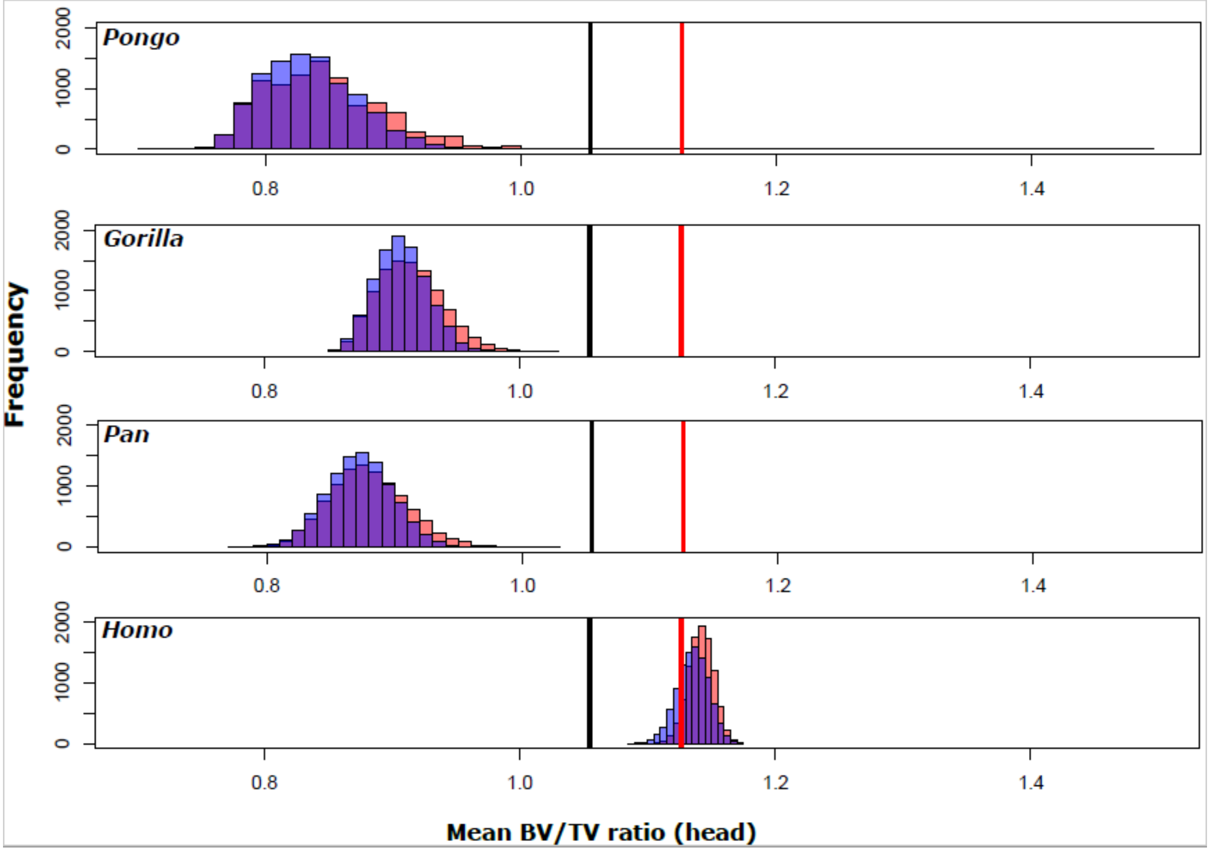

Figure 9. Bootstrap plots showing the sample means of BV/TV ratio within the head of each taxon. Pink bars represent the modern samples resampled and redistributed with SKX 5017; blue bars represent modern samples resampled and redistributed with SK 1813; purple bars represent overlap between the two samples. The red line represents the original BV/TV ratio of SKX 5017 and the black line represents the original BV/TV ratio of SK1813. The BV/TV ratio of SK 1813 falls outside the range of all taxa, with the exception of Pongo. The BV/TV ratio of SKX 5017 falls within the range of modern humans.

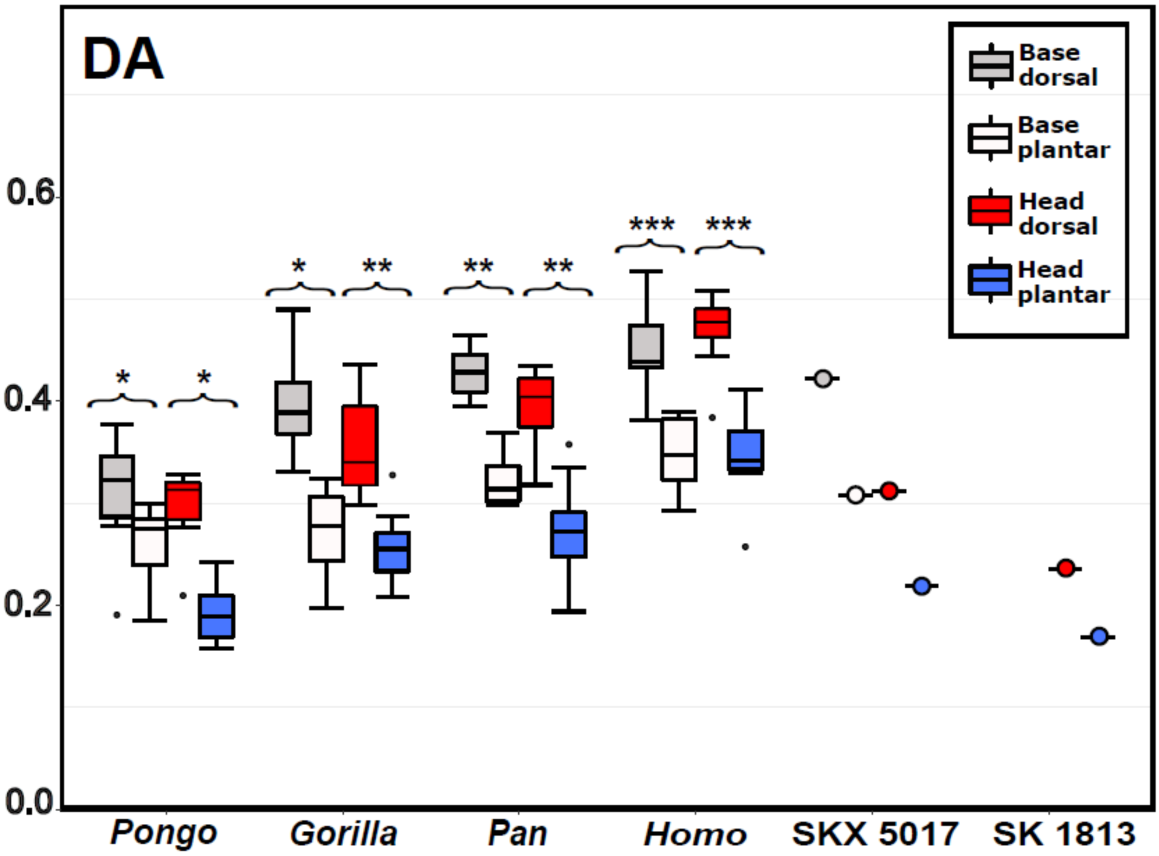

Figure 10. Boxplot showing raw DA values within each analysed region and each taxon. Significant differences in pairwise comparisons are denoted using asterisks (*) = $p<0.05$; (**) = $p<0.005$; (***) = $p<0.001$). All taxa display significantly higher DA in the dorsal regions of the element. Overall, modern humans show the absolute highest DA, and SK 1813 shows the lowest.

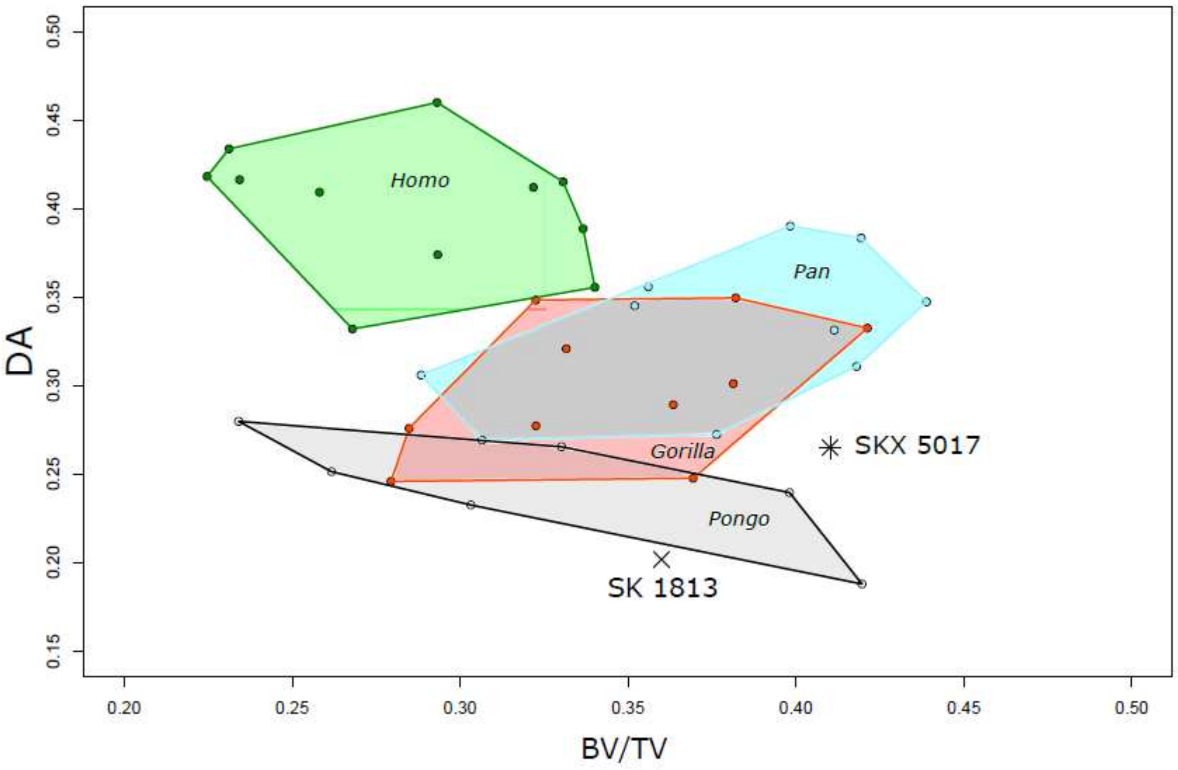

Figure 11. Scatterplot showing DA and absolute BV/TV values for the heads of all taxa. Dorsal and plantar regions have been combined to illustrate patterns in the entire epiphysis.

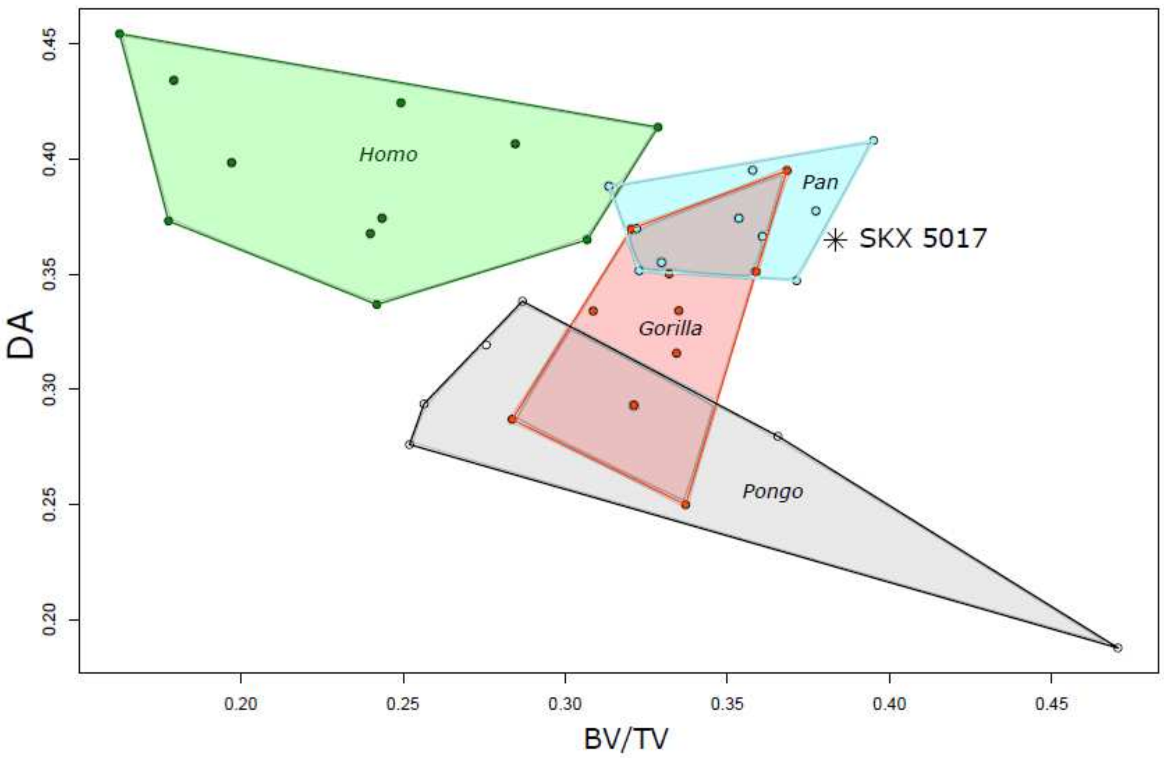

Figure 12. Scatterplot showing DA and absolute BV/TV values for the bases of all taxa. Dorsal and plantar regions have been combined to illustrate patterns in the entire epiphysis.